COMPUTATIONAL INVESTIGATION OF BUOYANCY EFFECT ON TEMPERATURE FIELD OVER AN AXISYMMETRIC MICROHEATER

By

SHANTANU SINGH

A THESIS PRESENTED TO THE GRADUATE SCHOOL
OF THE UNIVERSITY OF FLORIDA IN PARTIAL FULFILLMENT
OF THE REQUIREMENTS FOR THE DEGREE OF
MASTER OF SCIENCE

UNIVERSITY OF FLORIDA

2017

To my parents

ACKNOWLEDGMENTS

I would like to express my utmost gratitude to my advisor, Dr. Renwei Mei, Professor of Mechanical and Aerospace Engineering at University of Florida for his constant support, inspiration and encouragement. This dissertation would have been impossible without his expert guidance and enthusiasm on the subject.

I would also like to express my gratitude to Dr. David W. Hahn, chair of Mechanical and Aerospace Engineering and Dr. Jonathan R. Scheffe, Associate Professor of Mechanical and Aerospace Engineering for serving on my supervisory committee. I thank my fellow graduate students Mr. Amish Gadigi, Mr. Kelvin Randhir and Mr. Chen Chen for their immense support and encouragement. I also acknowledge the support provided by the High-Performance Computing Center at University of Florida.

Finally, I am deeply grateful for the enduring and endless support and love of my family.

TABLE OF CONTENTS

page

LIST OF TABLES

LIST OF FIGURES

LIST OF ABBREVIATIONS

Gr	Grashof number
Nu	Nusselt number
Pr	Prandtl number
Ra	Rayleigh number

LIST OF SYMBOLS

θ	Dimensionless temperature
Ψ	Stream function
ψ	Non-dimensional stream-function
Ω	Vorticity
ω	Non-dimensional vorticity
α	Thermal diffusivity
β	Coefficient of thermal expansion
T_{sat}	Saturation temperature
T_{wall}	Temperature of heater
υ	Kinematic Viscosity
η	Axial coordinate in computational domain
ξ	Radial coordinate in computational domain
a_a	Parameter in grid stretching
a_K	Parameter in grid stretching
γ	Parameter in grid stretching
α'	Parameter in grid stretching
β'	Parameter in grid stretching
ξ_0	Parameter in grid stretching
q^*	Dimensionless heat flux
λ	Constant for separation of variables
Q_{wall}	Heat flux on heater wall
R_∞	Infinite boundary in radial direction

Z_∞	Infinite boundary in axial direction
r	Radial coordinate
z	Axial coordinate
R	Non-dimensional radial coordinate
Z	Non-dimensional axial coordinate
u_r	Radial velocity
u_z	Axial velocity
U	Non-Dimensional radial velocity
V	Non-Dimensional axial velocity
x	Cartesian x coordinate
y	Cartesian y coordinate
ΔT	Degree of superheat
t	Dimensional time
t *	Non-dimensional time
p	Order of convergence
f_1	Flow field value for finest mesh
f_2	Flow field value for fine mesh
f_3	Flow field value for coarsest mesh
GCI	Grid convergence index

Abstract of Thesis Presented to the Graduate School
of the University of Florida in Partial Fulfillment of the
Requirements for the Degree of Master of Science

COMPUTATIONAL INVESTIGATION OF BUOYANCY EFFECT ON TEMPERATURE FIELD OVER AN AXISYMMETRIC MICROHEATER

By

Shantanu Singh

August 2017

Chair: Renwei Mei
Major: Mechanical Engineering

Steady state, laminar, external natural convection flow over a horizontal, circular, isothermal microheater is studied for Rayleigh number range up to 100 at Prandtl number of 1,5 and 10. Momentum and energy equations are solved using a finite-difference scheme for the fluid region over the heater. For the case of pure conduction; influence of domain size is studied and finite difference results are validated with the exact solution. Dependence of results on grid size is studied both for the case of pure conduction and convective flow. For conduction, grid dependency of results is checked against exact solution; whereas, for convective flow, Richardson extrapolation is used to check the results against extrapolated values. Finally, a correlation for dimensionless fluid temperature near the heater is developed as a function of dimensionless axial and radial coordinates, and Rayleigh number (θ (Z, R, Ra)). Least square regression fit is implemented to get the correlation. The correlation is a 4^{th} order unified polynomial valid for Rayleigh number from 0 to 100. Three correlations are developed for Prandtl number of 1,5 and 10. It is observed that the flow near the centerline of heater does not follow

boundary layer type behavior; whereas, it follows boundary layer type behavior on moving away from the centerline.

CHAPTER 1
INTRODUCTION

1.1 Background and Motivation

There are many application of boiling heat transfer, such as in high heat-flux electronic cooling, refrigeration, nuclear reactor cooling and in heat exchangers [1]. With a rapid rate of miniaturization of electronic components, there has been an ever-increasing demand to manage the high heat flux emanated from these compact devices. Presently, air-cooling is the most commonly used technique for electronic cooling; however, poor thermal transport properties of air reduces its potential for high heat flux thermal management. Boiling, on the other hand, is complemented by high heat transfer rate. Liquid immersion cooling involving boiling heat transfer, with dielectric fluids such as Fluorinert (FC series by 3M), is a pragmatic solution for cooling of microelectronics and microsystem packaging [2].

The phenomenon responsible for high heat transfer rate in boiling is bubble nucleation. It occurs when the surface is superheated and heat flux is below the critical heat flux. There have been many studies for bubble incipience on superheated surface. The conventional theory of nucleate boiling states that vapor/gas is trapped in imperfections (cavities and scratches) on a surface, which then serves as nuclei for bubble formation on superheated surface during boiling. Nucleation can be homogeneous or heterogeneous depending upon where bubble incipience occurs. If the bubble is formed in the bulk of liquid then nucleation is homogeneous, whereas if the bubble is formed at the fluid-superheated wall interface then it is a case of heterogeneous nucleation. In absence of trapped-vapor sources on the heating surface, homogeneous nucleation occurs at high wall superheats (homogeneous limit); while the

presence of trapped vapor sources on the surface results in heterogeneous nucleation, which occurs at relatively lower wall superheats (heterogeneous limit) [3] [4]. Theoretical and experimental studies conducted during the 1970s and 1980s suggested that the only mode of nucleation possible on cavity free surfaces was homogeneous nucleation [5] [6] [7]. The long held classic nucleation theory (CNT) of trapped-vapor giving rise to nucleation, was questioned in 2002 when Theofanous et al. [8] observed nucleation at low wall superheat, over a cavity-free surface (nanoscopic level smooth heater free of micron-scale cavities). Low wall superheat was supposed to be a characteristic of heterogeneous nucleation, a phenomenon which cannot occur on a cavity-free surface, according to the existing theory.

Subsequently, Qi and Klausner [9] were also able to initiate boiling at low wall superheats on nanoscopic level smooth stainless steel and brass surfaces. Bon et al. [10] evaluated the nucleation wall superheat of two fluids (pentane and Hexane) over nine types of different surfaces. They found these nucleation wall superheats to be 30 to 50 % of the homogeneous limit for all cases. Even more similar studies [11] [12] [13] [14] demonstrated heterogeneous nucleation at low wall superheats (~10 K under atmospheric water-saturated conditions) on a smooth hydrophilic surface. These experimental findings strengthened the opinion that heterogeneous nucleation could be found over smooth cavity-free surfaces devoid of vapor traps.

To explain the contradictions to the established nucleation theory, Jo et al. [15] in 2014 used a thermal boundary layer model. They combined their boundary layer model with kinetics and dynamics of superheated liquid and thermodynamic stability of generated vapor. Using a 2-D boundary layer approximation they arrived at temperature

field of exponential form. However, their solution was formulated over a semi-infinite smooth horizontal plate and they assumed the presence of thermal boundary layer.

Flows over microheater fall in low Ra range due to the small characteristic length of microheater. However, most of the studies done in this regard focused on high Ra range, wherein they predicted the existence of a well-developed boundary layer [16] [17]. Petralanda [3] solved a 3-D conduction problem over a heater and came up with a two-term simple correlation for temperature at centerline. However, influence of Ra was not clear.

Suriano et al. [18] studied steady, laminar natural convection on a semi-infinite plate for moderate Ra. They predicted a semi boundary layer type of behavior over the heater for Ra 300 onwards. Again, there study was for a semi-infinite plate. Therefore, a study of the temperature field over a finite geometry for low Ra range and different Pr would be helpful in describing the nature of flow over microheater.

1.2 Objective

Primary objective of the present research is to study the temperature field over a horizontal isothermal microheater due to a steady, laminar free convection flow over it. This study covers low Ra range up to 100. Correlation for temperature field of the form θ (Z, R, Ra) is to be obtained for Pr=1,5 and 10.

During nucleation, a bubble forms on top of the heating surface. It is worth noting that a temperature gradient exists from the heating surface to the bulk fluid in its vicinity. This fluid near the heater is at saturation temperature. Since the vapor embryo forms in the bulk liquid on top of the heating surface, the temperature gradient exists from the heater surface into the vapor bubble to all the way into the bulk fluid. It is

important to investigate this temperature gradient to understand the thermal boundary layer and deduce how it effects bubble incipience.

Moreover, cooling of a microelectronic device is an external flow natural convection problem for low range of Ra. Analysing the thermal field over the heater can reveal the dominant mode of heat transfer i.e. conduction or natural convection for these low Ra flows.

CHAPTER 2
LITERATURE REVIEW

2.1 Natural Convection over Isothermal Surfaces

Free convective boundary layer over isothermal surfaces have been extensively studied since 1958 [18] [16] [17] [19] [20]. Studies conducted by Stewartson [19] showed that only one of the two possible flows: heated plate facing upwards (or a cooled plate facing downwards), or a cooled plate facing upwards (or a heated plate facing downwards), would give rise to a boundary layer type of solution. Later Gill et al. [20] and Rotem [21] showed that boundary layer solution could only be obtained for the first case i.e. heated plate facing upwards (or a cooled one facing downwards). Petralanda [3] solved a 3-D conduction problem over a heater and came up with a two-term simple correlation for temperature at centerline. However, influence of Ra was not clear. Jo et al. [14] formulated an exponential temperature profile over a semi-infinite plate for natural convection case. They assumed 2 D boundary layer approximation.

Corcione [22] summarized the published experimental and numerical data on free convection from upward-facing horizontal plates. It was shown that there existed large variation in the heat transfer correlations because they were highly dependent on the surface geometry and fluid.

Temperature field is being investigated over a microheater. Now, Gr or Ra is directly proportional to x^3 and characteristic length (x) of microheater is in microns. Thus, flow over a microheater happens to be in low Ra range. Moreover, the previous studies assumed a semi-infinite geometry; whereas, finite size of the heater.is the focus of the present study.

2.2 Natural Convection for Low Ra

As explained in Section 2.1, small geometry results in low Ra flows, characterized by lower buoyancy forces and consequently lesser contribution by natural convection. Furthermore, past studies indicate the existence of threshold Ra in enclosed flows, below which natural convection does not occur.

According to the existing correlations, heat transfer due to natural convection increases with increasing Ra for external flows. However, Kostoglou et al. [23] showed that above is true only when Ra is above a threshold value. Below this value, there is no natural convection. Kostoglou et al. [24] studied a miniature spheroid heater with water and FC-72 as cooling fluid to ascertain the existence of threshold Ra for external flows. They predicted a threshold Ra value of 40 for water, while they were unable to determine a specific value for FC-72. They reported that Nu for FC-72 was insensitive to the Ra range of 400-1000, yet there would exist a threshold value for FC-72. The existence of low Gr and Ra sets this study in a unique region where the mode of heat transfer is not clearly defined.

Suriano et al. [18] carried out the study on horizontal plates for low Gr. Although their study was for a semi-infinite plate, nevertheless it can be insightful for analysis of finite geometry. They found that there was no effect of viscous dissipation on the flow physics**.** However, their conclusion was based on Pr=0.72 and 10, so the effect of dissipation on high Pr. fluid is still unclear.

Furthermore, they found three regions of interest based on the variation of Gr or Ra at constant Pr. The first region was for Ra up to unity, the second was for Ra up to 50 and the third for Ra up to 300. In first region, conduction was the only heat transfer mechanism. As the Ra increased into the second region, convection began to be

impactful; however, near the heating plate conduction was still more dominant. The Nu also started to increase beyond conduction. As the Ra was increased even further into the third region, boundary layer type flow started to develop**.** Authors predicted that the flow behaviour would gradually tend to boundary-layer type, as the Ra was increased beyond 300.

The present study will investigate low Ra flow over a flat plate type microheater for different Pr. The Ra range would be 0 to 100 and temperature field over microheater would be studied.

2.3 Domain Size for External Flows with Natural Convection

For flow over a microheater, the walls confining the flow are located at a scale much larger than the scale of the heater itself. Therefore, for flow over a microheater, the boundaries are essentially at infinity. Infinite boundaries have been a source of difficulty. For a semi-infinite plate, Suriano et al. [18] acknowledged from an analytical perspective that, analysis of infinite domain problem should be done by matching some near heater solution (analytical or numerical) to asymptotic solution at large distance from the heated surface. The only available asymptotic solution is the well-known boundary layer far wake solution, where the velocity component opposite to the gravity field increases unboundedly with the distance from the heating surface. This is not feasible physically and more so in the case of low Ra flows. To define the flow boundaries for their numerical studies, Suriano et al. chose a rectangular finite domain whose dimensional scale was large compared to the length scale of their heating surface.

Since then, many studies used the same concept of sufficiently large domain size to simulate the effect of infinite boundaries [24] [16] [25] [26].

In the present study, a finite domain size was chosen and grid stretching technique was implemented to efficiently resolve the high gradient region. It is to be noted that the flow field and temperature field near the heater are independent of domain size after a certain value of domain size, as will be explained later. So, we mainly focus our study on the region near heater bounded by R=1, Z=1, i.e. 1X1 domain.

CHAPTER 3
NUMERICAL MODELLING

3.1 Governing Equations

To model a steady, laminar, free convection external flow, a vertical cylindrical domain with the microheater in the bottom center was assumed. Generally, the heating element in boiling heat transfer experiments is a planar array of several microheaters arranged in a certain pattern [12] [27]. For studying a single bubble incipience, Chen et al [12] chose to keep only one of the 96 distinct microheaters active. Dimensions of a single microheater was taken as 250 µm X 250 µm in the study by Petralanda [3]. With such a size of microheater it is safe to say that; the length scale of domain size was large enough compared to the length scale of heater to make the domain an infinite boundary.

Figure 3-1 shows the schematic representation of the problem under study. The flow is axisymmetric and Boussinesq approximation is used in representing the buoyancy force. The stream function-vorticity formulation is used in lieu of Navier-Stokes equation. Due to axisymmetric nature of the flow, the modeling could be done in one-half of a 2-D axial plane as shown in Figure 3-2. Other assumptions employed are: negligible viscous dissipation [1], no heat generation, and constant fluid properties viz. thermal diffusivity (α), kinematic viscosity (υ) and volume expansion (β) [24].

With the use of stream function Ψ in cylindrical coordinates (r, z), the velocity can be evaluated as

$$u_r = -\frac{1}{r}\frac{\partial \Psi}{\partial z}, u_z = \frac{1}{r}\frac{\partial \Psi}{\partial r} \tag{3-1}$$

where u_r and u_z are the r and z-component of the fluid velocity, respectively. This ensures that the continuity equation is automatically satisfied. From the definition of vorticity, Ω, in axisymmetric flow, $\Omega = \frac{\partial u_r}{\partial z} - \frac{\partial u_z}{\partial r}$, the following relation is established:

$$\frac{\partial}{\partial r}\left(\frac{1}{r}\frac{\partial \Psi}{\partial r}\right) + \frac{1}{r}\frac{\partial^2 \Psi}{\partial z^2} = -\Omega \tag{3-2}$$

The momentum equations for u_z and u_r in the presence of buoyancy force is modeled using Boussinesq approximation, and it can be combined by cross-differentiation to obtain the vorticity transport equation:

$$\frac{\partial \Omega}{\partial t} + \frac{\partial (u_r \Omega)}{\partial r} + \frac{\partial (u_z \Omega)}{\partial z} = \upsilon\left[\frac{\partial^2 \Omega}{\partial r^2} + \frac{1}{r}\frac{\partial \Omega}{\partial r} - \frac{\Omega}{r^2} + \frac{\partial^2 \Omega}{\partial z^2}\right] - g\beta\frac{\partial T}{\partial r} \tag{3-3}$$

The energy equation for temperature *T* in the axisymmetric flow is:

$$\frac{\partial T}{\partial t} + \frac{\partial (r u_r T)}{r \partial r} + \frac{\partial (u_z T)}{\partial z} = \alpha\left(\frac{\partial^2 T}{\partial r^2} + \frac{1}{r}\frac{\partial T}{\partial r} + \frac{\partial^2 T}{\partial z^2}\right) \tag{3-4}$$

For a heater with radius L as characteristic length, the following dimensionless variables and parameters are introduced,

$$t^* = \frac{\alpha t}{L^2}, R = \frac{r}{L}, Z = \frac{z}{L}, \omega = \Omega\left(\frac{L^2}{\alpha}\right), V = \frac{u_z L}{\alpha}, U = \frac{u_r L}{\alpha}, \psi = \frac{\Psi}{L\alpha}, \theta = \left(\frac{T - T_{saturation}}{T_{wall} - T_{saturation}}\right)$$

The dimensionless relationship between velocity, stream function and vorticity becomes:

$$U = -\frac{1}{R}\frac{\partial \psi}{\partial Z}, V = \frac{1}{R}\frac{\partial \psi}{\partial R}, \omega = -\frac{\partial V}{\partial R} + \frac{\partial U}{\partial Z} \tag{3-5}$$

$$\frac{\partial^2\psi}{\partial R^2}-\frac{1}{R}\frac{\partial\psi}{\partial R}+\frac{\partial^2\psi}{\partial Z^2}=-\omega R \tag{3-6}$$

The dimensionless vorticity transport and energy equations becomes:

$$\frac{\partial\omega}{\partial t^*}+\frac{\partial(U\omega)}{\partial R}+\frac{\partial(V\omega)}{\partial Z}=\Pr\left[\frac{\partial^2\omega}{\partial R^2}+\frac{1}{R}\frac{\partial\omega}{\partial R}+\frac{\partial^2\omega}{\partial Z^2}-\frac{\omega}{R^2}\right]-Ra_L\Pr\frac{\partial\theta}{\partial R} \tag{3-7}$$

$$\frac{\partial\theta}{\partial t^*}+\frac{\partial(RU\theta)}{R\partial R}+\frac{\partial(V\theta)}{\partial Z}=\frac{\partial^2\theta}{\partial R^2}+\frac{1}{R}\frac{\partial\theta}{\partial R}+\frac{\partial^2\theta}{\partial Z^2} \tag{3-8}$$

Where Ra= $\frac{g\beta\left(T_{wall}-T_{saturation}\right)}{\upsilon\alpha}L^3$ and Pr= υ/α

3.2 Boundary Conditions and Grid Stretching

The boundary conditions were:

Z=0, $0\le R\le 1$; $\theta=1$

$1<R\le R_\infty$; $\theta=0$ (3-9a)

$0\le R\le R_\infty$; $\psi=\frac{\partial\psi}{\partial Z}=0$ (3-9b)

R=0, $0\le Z\le Z_\infty$; $\omega=\psi=\frac{\partial\theta}{\partial R}=0$ (3-9c)

R= R_∞, $0\le Z\le Z_\infty$; $\theta=\psi=\frac{\partial\psi}{\partial R}=0$ (3-9d)

Z=Z_∞, $0\le R\le R_\infty$; $\theta=\psi=\frac{\partial\psi}{\partial Z}=0$ (3-9e)

The first boundary condition of isothermal heater resulted in a temperature discontinuity. There was an option of giving the heater a constant heat flux condition or constant temperature condition. However, it is preferable to maintain the heaters at a constant temperature for the following reasons [3] [12] [27]

1. Maintaining a constant surface temperature of heater reduces the complexity of the analysis because it eliminates the spatial changes in wall temperature.
2. Conduction between adjacent microheaters through substrate is minimized as they are at the same temperature.
3. By eliminating conduction in the substrate and providing a constant-temperature boundary condition, numerical or analytical models of nucleate and transition boiling, and critical heat flux, can be simplified.
4. Data acquisition of critical heat flux and transition boiling regime can be done without the danger of heater dry out.
5. To identify the nature of boiling incipience a constant temperature condition is favoured because degree of superheat is a controlling parameter.

To accommodate for a large domain (large R_∞ and Z_∞) to reduce the impact of the domain size in the present study, grid stretching is necessary in R- and Z-directions. Furthermore, there is a discontinuity in boundary condition at the end of the heater; thus, smaller grid spacing is needed near R=1 to maintain a sufficient resolution.

A recirculating flow is expected within the enclosure of large but finite domain. However, upon increasing Ra a boundary-layer type flow could also be expected. In the case of a boundary layer flow, the thickness of the boundary layer decreases with an increase in Ra. To capture any boundary layer type of behavior, sufficient grid resolution should be maintained in the Z-direction near the heater. To simulate far-field boundaries, the length scale of domain size should be large enough than the length scale of heater. The characteristic length of a typical microheater is around 125 μm; which is practically negligible when compared to the radius of the vessel in which boiling

heat transfer experiment is carried out [3]. To define a domain, it was required to choose some value of R_∞ and Z_∞, so that an imaginary boundary wall at that position was sufficiently far enough not to affect the temperature field and flow pattern over microheater. Goldstein et al. [19] reported a mere increase of 2% in heat transfer rate on doubling the size of the domain. In the present study, the effect of different domain size was observed on local flow field over the heater as will be explained later in section 4.1. Accordingly, a domain size of 10 was chosen so that the results in 1X1 region were relatively independent of domain size.

The physical domain represented by R and Z were transformed to a computational domain represented by a uniformly spaced grid with dimensions ξ and η (0≤ ξ ≤1, 0≤ η ≤1). Following are the mathematical definitions of the grid:

In R-dimension:

$$R = \frac{\left(\xi + \frac{\alpha'}{3}\left((\xi-\xi_0)^3 + \xi_0^3\right)\right)}{\left(\xi_0 + \frac{\alpha'}{3}\xi_0^3\right)}, 0 \le R \le 1$$

$$R = 2 + a_a\left(e^{\gamma(\xi-2\xi_0)+a_K(\xi-2\xi_0)^2} - 1\right), 1 < R \le R_\infty \qquad (3\text{-}10)$$

where;

α', a_a is adjusted for proper grids; $a_K = \dfrac{\left(\ln\left(1+\dfrac{(R_\infty-2)}{a_a}\right) - \gamma(1-2\xi_0)\right)}{(1-2\xi_0)^2}$, ξ_0 =0.25 (3-11)

In Z-dimension:

$$Z = \frac{Z_\infty(1+\beta'\tan^{-1}((2\eta-1)\tan(1/\beta')))}{2} \qquad (3\text{-}12)$$

Parameter *β'* is adjusted for proper grids. Table 3-1 shows the value for grid stretching parameters used in the present study for different domain sizes.

The above grid stretching ensures that the boundary condition discontinuity at R=1 always falls between the two adjacent grids for all grid sizes as shown in Figure 3-3. Having the discontinuity halfway between two grids does not results in a loss of resolution on increasing the grid size by a given factor (2 in the present study).

3.3 Discretization Method

The stream function equation is elliptic; while, the vorticity-transport and energy equations are parabolic. To transform the physical grid to computational grids, following terms were defined:

$$h1_i = (\frac{\partial R}{\partial \xi})_i, h2_j = (\frac{\partial Z}{\partial \eta})_j$$

Equation (3-6) to (3-8) are written in conservative form and they are discretized using three-point central difference scheme. Vorticity and temperature field on internal grids were advanced across a time step from t^{*n} to t^{*n+1} using semi-implicit finite difference approximation to the above equations. The following discretization are implemented in the code in the given order:

$$\begin{aligned}
&\frac{\omega_{i,j}^{n+1} - \omega_{i,j}^{n}}{\Delta t^{*}} + \frac{(U_{i+1,j}\omega_{i+1,j}^{n} - U_{i-1,j}\omega_{i-1,j}^{n+1})}{(2\Delta\xi)} h1_i + \frac{(V_{i,j+1}\omega_{i,j+1}^{n} - V_{i,j-1}\omega_{i,j-1}^{n+1})}{(2\Delta\eta)} h2_j \\
&= \Pr\left[\begin{array}{l}
(\frac{h1_{i+1/2}\omega_{i+1,j}^{n} - (h1_{i+1/2} + h1_{i-1/2})\omega_{i,j}^{n+1} + h1_{i-1/2}\omega_{i-1,j}^{n+1}}{(\Delta\xi)^2}) h1_i + \frac{(\omega_{i+1,j}^{n} - \omega_{i-1,j}^{n+1})}{R_i(2\Delta\xi)} h1_i \\
+(\frac{h2_{j+1/2}\omega_{i,j+1}^{n} - (h2_{j+1/2} + h2_{j-1/2})\omega_{i,j}^{n+1} + h2_{j-1/2}\omega_{i,j-1}^{n+1}}{(\Delta\eta)^2}) h2_j - \frac{\omega_{i,j}^{n+1}}{R_i^2}
\end{array}\right] \\
&- Ra_L \Pr \frac{(\theta_{i+1,j}^{n} - \theta_{i-1,j}^{n+1})}{(2\Delta\xi)} h1_i
\end{aligned} \tag{3-13}$$

$$\frac{\theta_{i,j}^{n+1}-\theta_{i,j}^{n}}{\Delta t^{*}}+\frac{(R_{i+1}U_{i+1,j}\theta_{i+1,j}^{n}-R_{i-1}U_{i-1,j}\theta_{i-1,j}^{n+1})}{R_i(2\Delta\xi)}h1_i+\frac{(V_{i,j+1}\theta_{i,j+1}^{n}-V_{i,j-1}\theta_{i,j-1}^{n+1})}{(2\Delta\eta)}h2_j$$
$$=(\frac{h1_{i+1/2}\theta_{i+1,j}^{n}-(h1_{i+1/2}+h1_{i-1/2})\theta_{i,j}^{n+1}+h1_{i-1/2}\theta_{i-1,j}^{n+1}}{(\Delta\xi)^2})h1_i+\frac{(\theta_{i+1,j}^{n}-\theta_{i-1,j}^{n+1})}{R_i(2\Delta\xi)}h1_i \qquad (3\text{-}14)$$
$$+(\frac{h2_{j+1/2}\theta_{i,j+1}^{n}-(h2_{j+1/2}+h2_{j-1/2})\theta_{i,j}^{n+1}+h2_{j-1/2}\theta_{i,j-1}^{n+1}}{(\Delta\eta)^2})h2_j$$

$$(\frac{h1_{i+1/2}\psi_{i+1,j}^{n}-(h1_{i+1/2}+h1_{i-1/2})\psi_{i,j}^{n+1}+h1_{i-1/2}\psi_{i-1,j}^{n+1}}{(\Delta\xi)^2})h1_i-\frac{(\psi_{i+1,j}^{n}-\psi_{i-1,j}^{n+1})}{R_i(2\Delta\xi)}h1_i$$
$$+(\frac{h2_{j+1/2}\psi_{i,j+1}^{n}-(h2_{j+1/2}+h2_{j-1/2})\psi_{i,j}^{n+1}+h2_{j-1/2}\psi_{i,j-1}^{n+1}}{(\Delta\eta)^2})h2_j=-\frac{\omega_{i,j}^{n+1}}{R_i} \qquad (3\text{-}15)$$

At the boundary, new vorticities are calculated from the stream function boundary condition as stated in Section 3.2. A first order vorticity approximation is obtained by combination of Taylor series expansion for ψ near the wall, and the boundary conditions for the derivative of ψ. For instance, vorticity at bottom wall is calculated by Eq. (3-16)

$$\omega_{i,j}^{n+1}=-\frac{2\psi_{i,j+1}^{n+1}}{R_i(\Delta\eta)^2}h2_j^2 \qquad (3\text{-}16)$$

Now we define the dimensionless heat flux at the heater surface q*(ξ) as:

$$q^{*}(\xi)=\left.\frac{\partial\theta}{\partial\eta}\right|_{\eta=0} \qquad (3\text{-}17)$$

The iterative solutions were converged when the L2 norm for heat flux and vorticity at the bottom wall, defined by Eq. (3-18) and (3-19), became less than 10^{-10}.

$$L_2(q^{*})=\sqrt{\frac{\sum_{i=1}^{nx}(q_i^{*n+1}-q_i^{*n})^2}{\sum_{i=1}^{nx}(q_i^{*n})^2}} \qquad (3\text{-}18)$$

$$L_2(\omega)=\sqrt{\frac{\sum_{i=1}^{nx}(\omega_i^{n+1}-\omega_i^{n})^2}{\sum_{i=1}^{nx}(\omega_i^{n})^2}} \qquad (3\text{-}19)$$

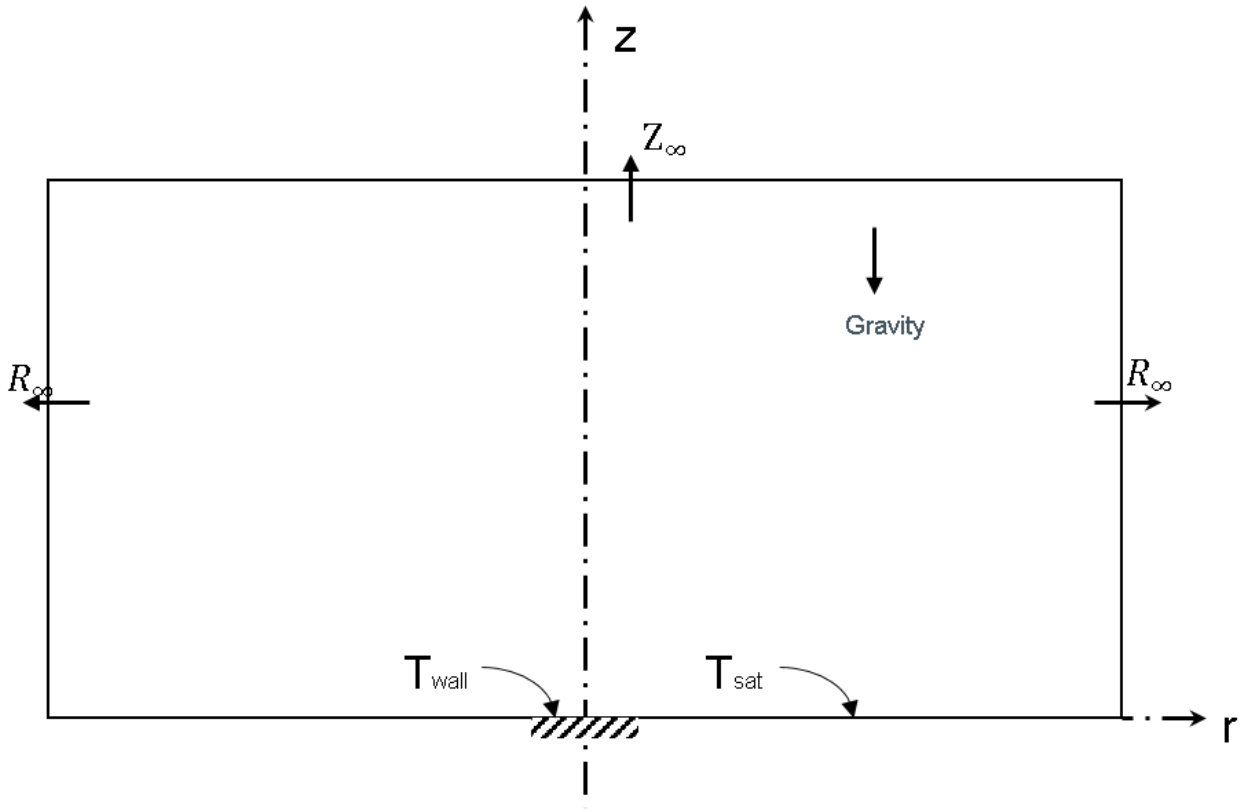

Figure 3-1.Sectional view of cylindrical domain over an axisymmetric microheater with cylindrical coordinate system

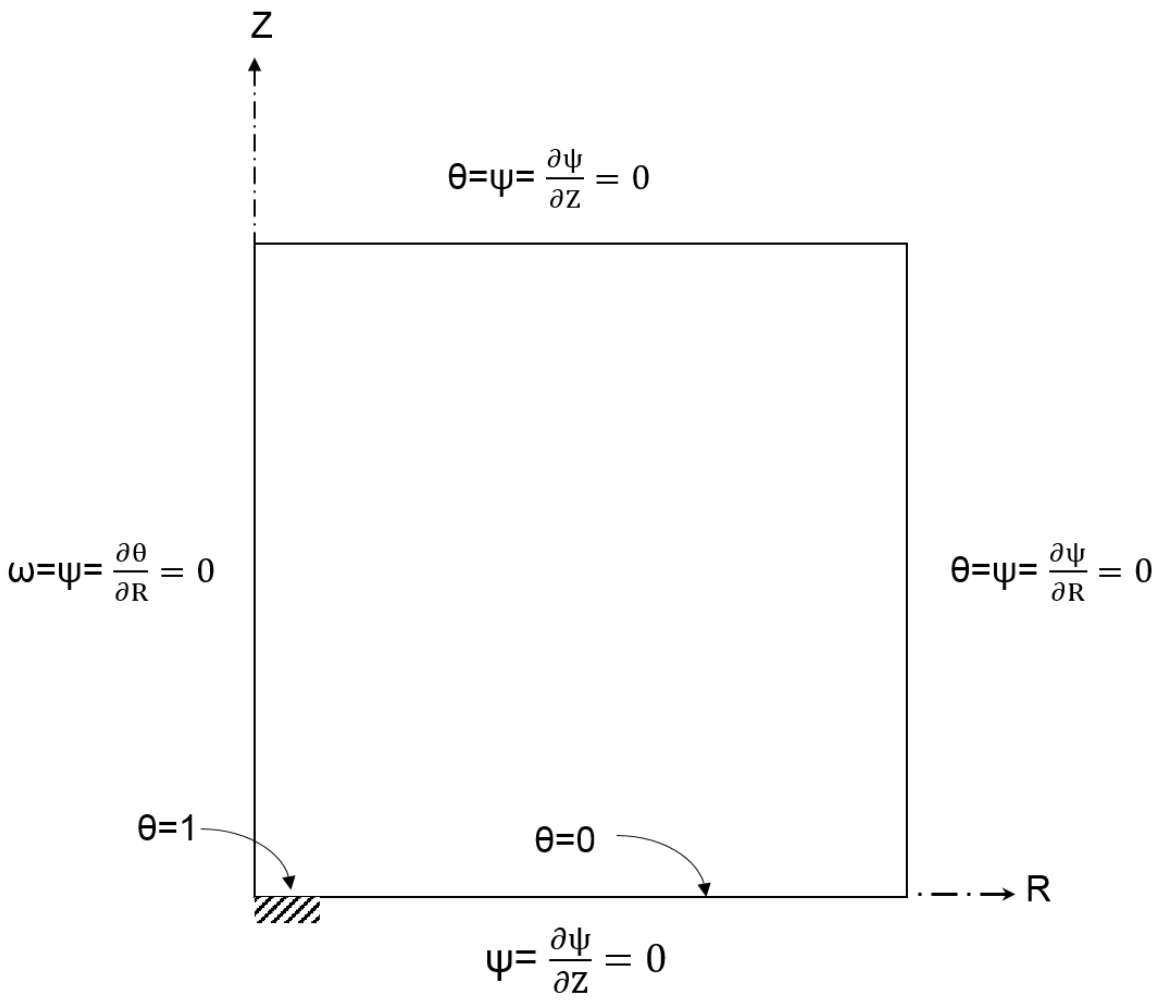

Figure 3-2. 2 D axisymmetric axial plane with boundary conditions

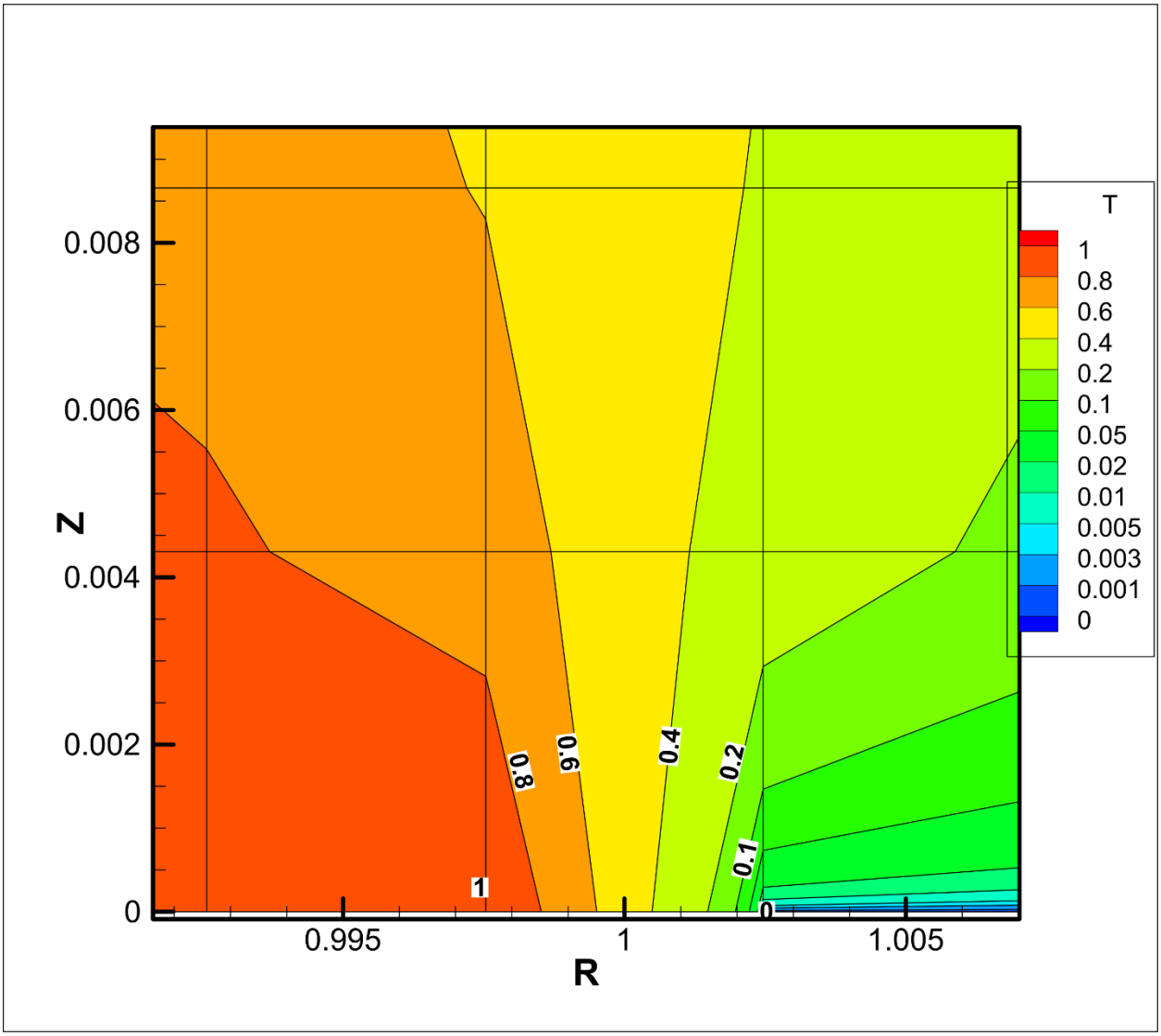

Figure 3-3. The point of discontinuity R=1 is halfway between the two grids for all grid sizes (161X401 is the present grid)

Table 3-1. Grid stretching parameters for different domain size

	R=Z=10	R=Z=50	R=Z=100
a_a	51.7	51.7	51.7
ξ_0	0.25	0.25	0.25
β'	0.75	0.70	0.94
α'	188	188	188

CHAPTER 4
RESULTS AND DISCUSSIONS

4.1 Influence of Domain Size

To simulate the effect of an infinite boundary a finite domain size should be chosen such that increasing the size any further does not produce any meaningful change in the flow field near heater. For this purpose, results were generated using domain size of 10,50 100, for the case of pure conduction. Figure 4-1 (a), (b) and (c) show that finite difference temperature solution for domain size R=10,50 and 100 follows the exact solution of temperature very closely, for a range of R values between 0 to 1. It is evident that increasing the domain size further than 10 had no considerable influence on the flow physics in the 1X1 region over heater. Based on above analyses, it is safe to conclude that $R_\infty = Z_\infty = 10$ is a well enough domain size. to represent boundaries at infinity. Figure 4-2 shows isotherms over heater for various domain sizes. It was observed that the isotherms pattern remained unaffected by a change in domain size.

With a proper choice of modelling parameters, the code was implemented to generate results. Following methods were used for validation of numerical modelling results:

1. Comparing exact temperature solution with finite difference results for pure conduction case.
2. Comparing available experimental results and modelling results.

It is worth mentioning that patterns in entire computational domain were compared with reported literature only for validation. It was known that the results far away from heater are domain size dependent, so they were of no physical significance.

For the present study, it is only the results in vicinity of heater that matters. However, obtaining a similar streamline and isotherm pattern to that of reported literature would attest the validity of our modelling.

4.1.1 Validation Based on Exact Solution for Pure Conduction Case

Energy equation for pure conduction in cylindrical coordinates reduces to Eq. (4-20).

$$\frac{1}{R}\frac{\partial}{\partial R}\left(R\frac{\partial\theta}{\partial R}\right)+\frac{\partial^2\theta}{\partial Z^2}=0 \tag{4-20}$$

Boundary Conditions:

$Z=0,\ 0\le R\le 1;\quad \theta=1$

$1<R\le\infty;\quad \theta=0$ (4-21a)

$Z\to\infty:\ \theta(R\ Z)=0$ (4-21b)

$R=0:\ \frac{\partial\theta}{\partial R}=0$ (4-21c)

$R\to\infty:\ \theta(R\to\infty, Z)=0$ (4-21d)

Solution for the above case is of form:

$$\theta(R,Z)=\int_0^\infty c(\lambda)e^{-\lambda Z}J_0(\lambda R)d\lambda \tag{4-22}$$

Using Eq. (4-21a, b, c, d) the following solution is obtained:

$$\theta(R,Z)=\int_0^\infty J_1(\lambda)e^{-\lambda Z}J_0(\lambda R)d\lambda \tag{4-23}$$

At the centerline R=0, therefore Eq.(4-23) becomes

$$\theta(Z)=\int_0^\infty J_1(\lambda)e^{-\lambda Z}d\lambda \tag{4-24}$$

Numerical integration is used to get the θ(Z). The above equations were used to generate exact solution for different values of R.

To observe accuracy of finite difference solution and the effect of domain size; finite difference solution of temperature θ(Z) obtained by different domain sizes (R_∞ = Z_∞ =10,50.100) were compared with the generated exact solution for the respective R values.

Figure 4-1 (a), (b), (c) shows the comparison between exact solution and finite difference results for domain sizes of 10,50,100. Finite difference results for different domain sizes followed the exact solution closely for a range of R values between 0 to 1. Moreover, the agreement between finite difference results and exact solution goes even up to Z =2. From the above observation, the following is concluded:

1. The code is validated for pure conduction case.
2. Domain sizes of 10, 50 and 100 produce similar temperature field near heater. Therefore, further discussions are based on results produced by domain size of 10.

4.1.2 Validation Based on Comparison of Experimental and Numerical Isotherms and Streamlines

Torrance and Rockett [28] used an identical mathematical model for study of natural convection in a cylindrical enclosure. They studied natural convection over a heater for a range of Gr, with air as the fluid (Pr=0.7). They used a normalized domain size of 1X1 with length of heater as 0.1. The domain used in present study was 10X10 with heater length of 1; therefore, result of the present study are scaled by a factor of 10.

To validate the results of present study by comparing with the results of Torrance and Rockett, we scaled the Gr and Ra in proportion to domain size ratio of the two studies. Length ratio of the domain size in two studies was 10. Since the Gr is directly

proportional to L^3, equivalent Gr in this study would be a thousandth of that used by Torrance et al. Torrance et al. [29] also conducted experimental studies for Pr=0.7.

Results were generated for Pr=0.7 in the present study and they were compared to the existing literature. For a comparison with reported experimental results, modelling was done for Pr=0.7 with Gr=800 or Ra=560 ($Gr=8X10^5$ for reported literature). Figure 4-3 shows a good agreement between the experimental and numerical modelling. The streamline patterns were in good agreement.

This code was also run for the case of conduction and Gr= 40 or Ra=28($Gr=4X10^4$ for reported literature), to compare our numerical results to the numerical results in existing literature [28]. Figure 4-4 shows a good agreement between the two.

A validation based on value and position of ψ_{max} was also done. The results for Pr=0.7 and Ra=28, showed that the value of ψ_{max}=7.071 and it occurred at R= 4.938, Z=5.422. When scaled to compare with the results of Torrance et al. we get a value of ψ_{max}=0.707 occurring at R= 0.4938, Z=0.5422. Torrance reported a value of ψ_{max}=0.719 and it occurred at almost R=Z=0.5; thus, the obtained results are in close agreement with reported literature.

4.2 Influence of Grid Size

4.2.1 Iterative Convergence

Equations (3-18) and (3-19) were used to check the iterative convergence as explained in section 3.3. Often false convergence results when there is a momentary plateau in convergence curve for a span of iterations. To avoid this, convergence was not checked after every iteration for the whole iterative process. Instead, following criterion was implemented for convergence check **:** for iteration range 0 to 5,000 ,

convergence was checked after every iteration; for iteration range 5,000 to 50,000 , convergence was checked after every 20 iterations; for iteration range 50,000 to 500,000 , convergence was checked after every 100 iterations; for iteration range 500,000 to 3,000,000 , convergence was checked after every 1000 iterations and for iterations above 3,000,000 , convergence was checked after every 10,000 iterations. Figure 4-5 shows the residual plot for the iterative convergence for Pr=10, Ra=28. Once the convergence criteria for both type of residuals goes under 10^{-10}, steady state was achieved. Thus, the results can be assumed to be steady with respect to iterations of time.

4.2.2 Grid Convergence for the Case of Pure Conduction

The code used in present study implemented grid interpolation to advance the result on a specific grid system as an initial condition for the next finer grid size. Grid refinement was done by a factor of two. Thus, mesh size was refined from 41X101 to 81X201 to 161X401 to 321X801.

Finite difference temperature solution obtained by different grid size were compared to exact solution for pure conduction case. $\theta(R)$ up to $R<2$ was plotted for various locations of Z. Figure 4-6 shows the comparison. It is observed that even till Z=2 and R=2, results from grids 81X201, 161X401 and 321X801 are similar and follow the exact solution very closely. Thus, the results can be considered converged with respect to grid size at grid size of 161X401 for pure conduction case and we can save the additional computational cost required in case of 321X801 grids.

4.2.3 Grid convergence for Moderate Convective Flow

For Ra=100 and Pr=1; grid convergence study using Richardson's extrapolation was carried out, and flow filed values at various locations of the domain were compared with the respective extrapolated values. Eq. (4-25) and (4-26) are used for extrapolation

$$p = \frac{\ln\left(\frac{f3 - f2}{f2 - f1}\right)}{\ln(r)} \tag{4-25}$$

$$f_{extrapolated} = f_3 - \left(\frac{f_3 - f_2}{2^p - 1}\right) 2^p \tag{4-26}$$

Where, p is order pf accuracy

f1, f2, f3 are the flow field values for mesh size 1,2,3 with 1 being the finest and 3 most coarse

r is the grid refinement ratio which is 2 for present case

For different grid sizes, values of finite difference vorticity, stream-function, theta, radial and axial velocities were compared with extrapolated values for the case of Pr=1 and Ra=100. Table 4-1 shows the grid convergence and order of accuracy analysis for a specific location R=1 and Z= 0.026471. Results show that the deviation between extrapolated values and finite difference values given by 161 X 401 grids is very less. Moreover, the local order of accuracy is close to 2.

Another similar analysis was conducted at radial location R=0 i.e. centerline and R=0.7, for Z going from 0 to 1. At R=0, local order of accuracy of temperature was calculated for the axial grid locations common in 81X201, 161X401 and 321X801 grids. Error and Grid convergence index (GCI) between the grids were also calculated using Eq.(4-27) and (4-28). As defined by Roache [30], GCI provides an estimate of the discretization error in finest grid solution relative to the converged numerical solution.

The converged numerical solution lies in the interval [f_1(1-GCI),f_1(1+GCI)] with a 95 % confidence level for a typical factor of safety Fs=1.25

$$e_{21} = \left| \frac{f_2 - f_1}{f_2} \right| \tag{4-27}$$

$$GCI_{21} = F_s \frac{e_{21}}{r_{21}^p - 1} \tag{4-28}$$

Where, e_{21} is error between grids 161X401 and 321X801

F_s is factor of safety (1.25 in present study)

r_{21} is grid refinement ratio between grids 161X401 and 321X801 (2 in present study)

p is order of convergence

GCI_{21} is the grid convergence index between grids 161X401 and 321X801

Table 4-2 shows the local order of accuracy and GCI for temperature at R=0 with respect to Z locations (Z<1). It is observed that the local order of accuracy is almost 2 which is consistent with the discretization scheme used to model the study. Moreover, GCI21 and GCI32 are significantly small; suggesting that: even results obtained by grids 161X401 are almost as accurate as extrapolated solution. Figure 4-7 and Figure 4-8 shows that all the grid sizes considered in the present study follow the extrapolated solution closely at location R=0 and R=0.7. Based on above analyses for conduction and convection case, it is observed that results from 161X401 are sufficiently accurate and they can be considered converged with respect to grid size. Therefore, further results are based on a grid size of 161X401.

4.3 Results

Present study covers a range of Ra from 0 to 100 for the fluid Pr of 1 ,5 and 10. The domain size, heater position and grid layout was as explained in the preceding text. Objective was to develop a correlation for the temperature field over microheater.

4.3.1 Effects of Pr and Ra on Steady State Isotherm and Streamlines

As explained in Section 4.1.2, it was only to show the similarity with the previous reported literatures that the isotherms and streamlines pattern in the whole domain were presented. Even though the numerical values outside 1X1 domain cannot be relied upon, yet observing the whole domain gives us an idea about the nature of flow.

Figure 4-9, Figure 4-10 and Figure 4-11 shows steady state isotherms and streamlines plotted for Pr=1 and Pr=10 with Ra=$1X10^{-8}$,28,50,75 and 100. Streamlines were plotted as ratio ψ/ψ_{max}. It was observed that the flow pattern formed a rolling vertex, whose center was approximately at R=Z=5, with ψ_{max} at the center. Table 4-3 shows the variation in value and position of ψ_{max} with respect to Ra. Circulation of fluid became stronger as ψ_{max} increased with Ra. It was observed that with an increase in Ra the vortex center gradually moves up with the radial position remaining almost same. Although there is only subtle difference between streamline pattern for conduction and Ra=100, but a numerical observation showed that the streamlines near the centerline, top of domain and right-hand side of domain moved closer to each other. Reason of this observation was higher velocities in these regions as Ra was increased.

When the fluid gets heated it formed a circulation pattern over heater. A rising column of hot fluid forms over the heater (near centerline). When this rising column encounters the boundary at infinity, the warm layer of fluid turns along the top boundary in form of a wall jet to flow radially. This moving fluid was once again turned by the wall

at $R=R_\infty, Z=Z_\infty$. The momentum of descending fluid maintains its motion despite of the retarding effect of buoyancy. As the fluid slows down it is entrained towards the heater once again and the height to which it rises is decided by it residual buoyancy.

For Pr=10, temperature at centerline, i.e. θ (Z, R=0) was observed for different Ra. Figure 4-12 shows that for a given Pr; the temperature profile becomes less steep. with an increase in Ra. Upon increasing Ra, convection increases and the fluid is moving upwards away from the heater wall making the temperature profile less steep. This phenomenon at centerline cannot be described by any conventional boundary layer theory, suggesting the absence of boundary layer behavior near centerline.

To see the influence of Pr when Ra is fixed; temperature profile at different radial locations were plotted for Pr=1 and 10 with Ra=100. From Figure 4-13 it is observed that temperature gradient in Z direction is steeper for the case of lower Pr i.e. 1 for R<0.3, whereas a steeper temperature gradient occurs for higher Pr i.e. 10 for R>0.3. For region 0.3<R<1, the flow is dominated by horizontal flow component and we observe a steeper temperature gradient for a flow with less thermal diffusivity (larger Pr), a behavior which can be described by boundary layer theory. For 0<R<0.3, steeper temperature gradient is observed for a high thermal diffusivity flow (lower Pr), a phenomenon which cannot be explained by boundary layer theory because in this region the flow turns direction and the vertical component of flow dominates. The above suggest that near the center a boundary layer type behavior does not exists.

4.3.2 Developing Correlation for Thermal Field near the Heater

A Taylor series expansion of θ(Z) on the heater for a given R value results in equation of form (4-29) or (4-30). Upon the heater (Z=0, 0≤R≤1), $\frac{\partial \theta}{\partial R} = \frac{\partial^2 \theta}{\partial R^2} = 0$ because

θ=1 for the heater. Using this result in Eq. (3-8) gives $\frac{\partial^2\theta}{\partial Z^2}=0$. Therefore, coefficient of Z^2 is zero in Eq. (4-29) or (4-30). From the finite difference results a correlation for θ (Z, R, Ra) of the form of Eq. (4-29) or (4-30) was developed. Following procedure was implemented to develop the correlation.

For each Pr=1,5 and 10; data was generated for Ra=0,14,28,36,50,63,75,90,100

For a given Pr:

1. For any particular Ra; θ(Z) given by finite difference was fitted by least square regression using MATLAB 2016a, to get an equation of form: $\theta\ (Z,\ given\ R)$ =1+$a_1\ Z$+$a_3\ Z^3$+ $a_4\ Z^4$. This process was done for various radial locations within the heater.

2. The same process is repeated for Ra=0,14,28,36,50,63,75,90,100. Thus, we get coefficient a_1, a_2, a_3 for a combination of different R and Ra as shown in Table 4-4, for a Pr=1.

3. For the data of form of Table 4-4, a 4th order multivariable regression was done in MATLAB using least square regression to develop correlation of form (4-29) or (4-30).

The same process was repeated to get correlation for thermal field near the heater for Pr=1,5 and 10. The correlation is valid for R<0.7 as beyond this region there is significant effect of strong singularity present at R=1.

The adjusted R square value was almost 0.998 or greater for all the fits thereby suggesting a good fit.

$$\theta(Z,\ given\ R_i) = 1 + \frac{\partial\theta}{\partial Zwall}\ Z + b_3 Z^3 + b_4 Z^4 \tag{4-29}$$

$$\theta(Z,R,Ra) = 1 + b_1(R,Ra)Z + b_3(R,Ra)Z^3 + b_4(R,Ra)Z^4 \tag{4-30}$$

Equations (4-31), (4-32) and (4-33) are the correlation for thermal field near heater (0≤Z≤1;0≤R≤0.7) for Pr of 1,5 and 10 valid for Ra range of 0 to 100.

$$\theta(Z,R,Ra)=1+(-0.99967+0.02436R+1.03767R^3-0.00794R^2Ra-1.00728R^2+0.00326Ra-1.16X10^{-7}RRa^2+4.01X10^{-7}Ra^3+0.00033RRa-4.50X10^{-5}Ra^2-1.77482R^4+0.00175R^3Ra+1.62X10^{-5}R^2Ra^2-1.53X10^{-8}RRa^3-1.45X10^{-9}Ra^4)Z+(0.54707-0.21405R-7.04261R^3+0.00426R^2Ra+3.82002R^2-8.79X10^{-5}Ra+3.48X10^{-7}RRa^2-1.36X10^{-7}Ra^3-0.00005RRa+1X10^{-5}Ra^2+9.99166R^4+0.00716R^3Ra-2X10^{-5}R^2Ra^2+2.93X10^{-8}RRa^3+5.68X10^{-10}Ra^4)Z^3+(-0.25541+0.19213R+6.14613R^3-0.00020R^2Ra-2.99156R^2-0.00062Ra-1.05X10^{-6}RRa^2+3.81X10^{-8}Ra^3-0.00011RRa-1.25X10^{-7}Ra^2-8.39982R^4-0.00719R^3Ra+1.20X10^{-5}R^2Ra^2-1.46X10^{-8}RRa^3-2.05X10^{-10}Ra^4)Z^4 \quad (4\text{-}31)$$

$$\theta(Z,R,Ra)=1+(-0.99766+0.01327R+0.98234R^3-0.00888R^2Ra-0.97260R^2+0.00312Ra-1.35X10^{-5}RRa^2+3.54X10^{-7}Ra^3+0.00112RRa-4.09X10^{-5}Ra^2-1.75018R^4+0.00274R^3Ra+4.40X10^{-6}R^2Ra^2+5.15X10^{-8}RRa^3-1.20X10^{-9}Ra^4)Z+(0.54408-0.21836R-7.04971R^3+0.00199R^2Ra+3.84435R^2+0.00146Ra+5.79X10^{-6}RRa^2+1.14X10^{-6}Ra^3+8.62X10^{-5}RRa-6.60X10^{-5}Ra^2+9.98243R^4+0.00851R^3Ra+1.09X10^{-5}R^2Ra^2-4.07X10^{-8}RRa^3-5.90X10^{-9}Ra^4)Z^3+(-0.25381+0.20140R+6.18710R^3+0.00221R^2Ra-3.03291R^2-0.00174Ra-7.29X10^{-7}RRa^2-9.26X10^{-7}Ra^3-0.00056RRa+5.70X10^{-5}Ra^2-8.40976R^4-0.00882R^3Ra-1.14X10^{-5}R^2Ra^2+2.18X10^{-8}RRa^3+4.68X10^{-9}Ra^4)Z^4 \quad (4\text{-}32)$$

$$\theta(Z,R,Ra)=1+(-0.99924+0.01154R+0.96664R^3-0.01041R^2Ra-0.95678R^2+0.00343Ra-1.97X10^{-5}RRa^2+4.24X10^{-7}Ra^3+0.00134RRa-4.68X10^{-5}Ra^2-1.73908R^4+0.00298R^3Ra+1.47X10^{-5}R^2Ra^2+9.57X10^{-8}RRa^3-1.60X10^{-9}Ra^4)Z+(0.54664-0.20942R-7.03639R^3+0.00431R^2Ra+3.81264R^2-0.00018Ra+1.83X10^{-5}RRa^2-3.43X10^{-7}Ra^3-0.00064RRa-2.48X10^{-5}Ra^2+9.98121R^4+0.00883R^3Ra-9.83X10^{-6}R^2Ra^2-9.72X10^{-8}RRa^3+1.55X10^{-9}Ra^4)Z^3+(-0.25529+0.19457R+6.18723R^3+0.00082R^2Ra-3.01390R^2-0.00058Ra-9.23X10^{-6}RRa^2+1.83X10^{-7}Ra^3-1.02X10^{-5}RRa-1.04X10^{-5}Ra^2-8.41719R^4-0.00920R^3Ra+2.47X10^{-6}R^2Ra^2+5.34X10^{-8}RRa^3-8.75X10^{-10}Ra^4)Z^4 \quad (4\text{-}33)$$

4.3.3 Verification of Correlation

To test the results of correlation in domain 0≤Z≤1;0≤R≤0.7 the following technique was used:

- For Pr=10, any random Ra=55(say) was taken and θ(Z) given by finite difference was compared to θ(Z) obtained by correlation at R=0.4, 0.5,0.6 and 0.7. Figure 4-14 shows the comparison.
- From Eq. (4-29) and (4-30) it is observed that wall heat flux is the coefficient b_1 itself. Thus, in Table 4-5 we compare the coefficient b_1 with the wall heat

flux obtained by finite difference, for various values of R for the case of Pr=10, Ra=28.

Both Figure 4-14 and Table 4-5 shows the that the temperature obtained by correlation follows the finite difference temperature results closely.

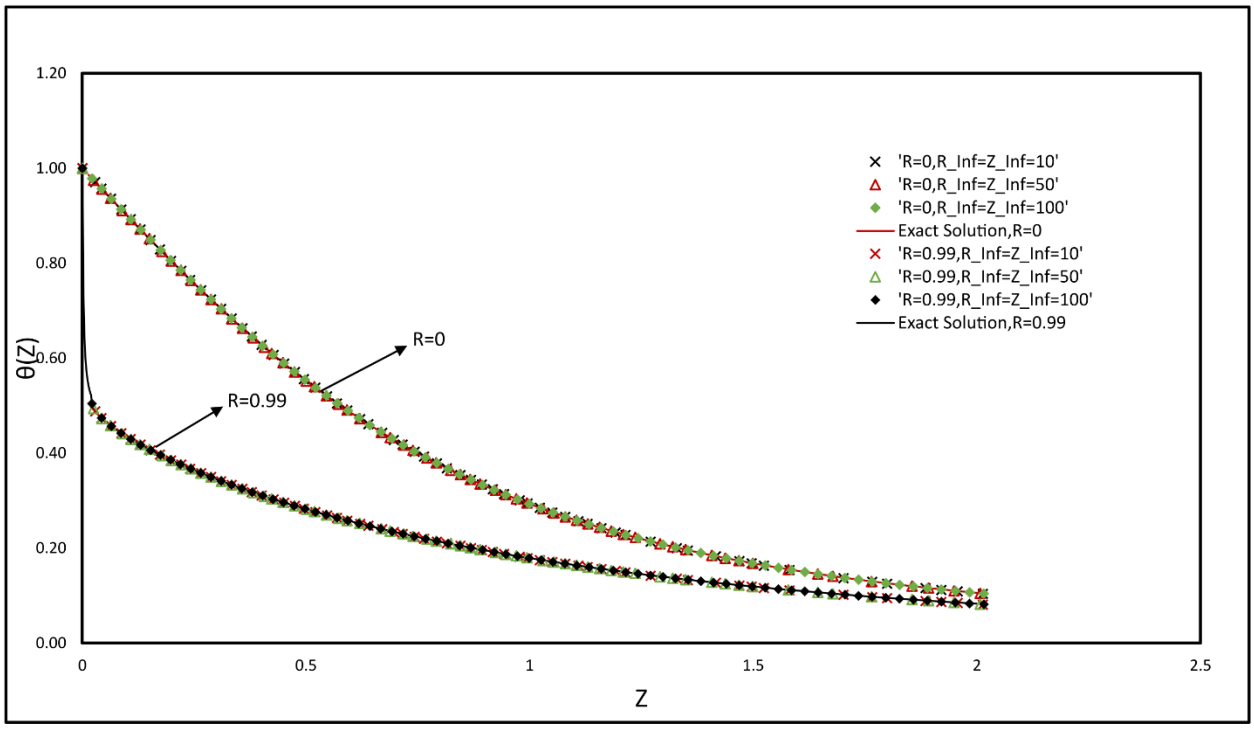
1.20
1.00
0.80
0.60
0.40
0.20
0.00
θ(Z)
0
0.5
1
1.5
2
2.5
Z
R=0
R=0.99
'R=0,R_Inf=Z_Inf=10'
'R=0,R_Inf=Z_Inf=50'
'R=0,R_Inf=Z_Inf=100'
Exact Solution,R=0
'R=0.99,R_Inf=Z_Inf=10'
'R=0.99,R_Inf=Z_Inf=50'
'R=0.99,R_Inf=Z_Inf=100'
Exact Solution,R=0.99

(a)

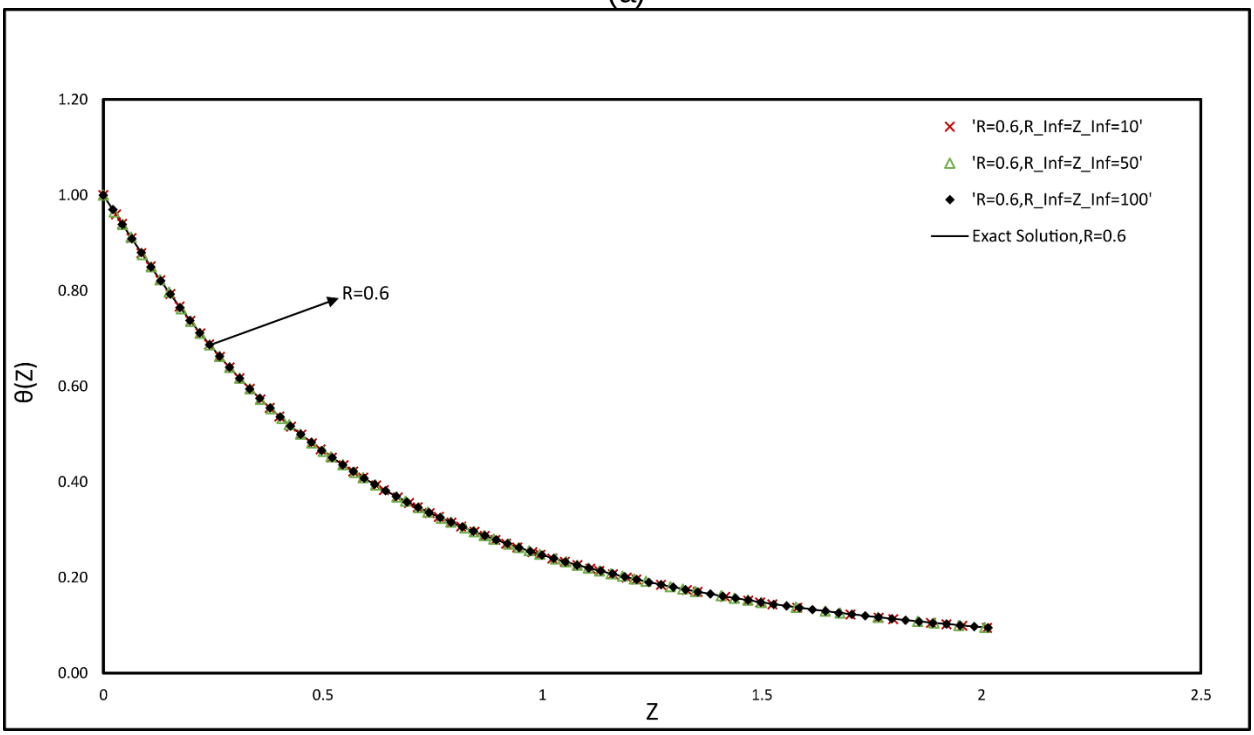
1.20
1.00
0.80
0.60
0.40
0.20
0.00
θ(Z)
0
0.5
1
1.5
2
2.5
Z
R=0.6
'R=0.6,R_Inf=Z_Inf=10'
'R=0.6,R_Inf=Z_Inf=50'
'R=0.6,R_Inf=Z_Inf=100'
Exact Solution,R=0.6

(b)

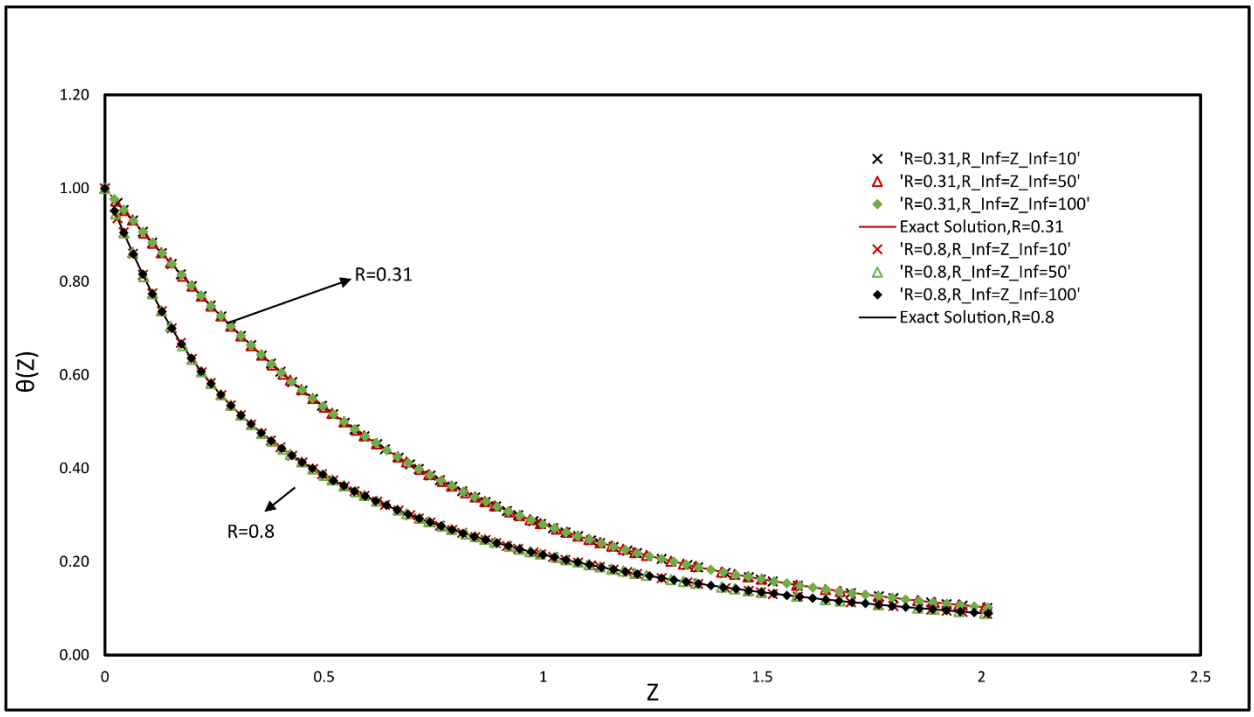

(c)

Figure 4-1.Comparison between exact solution of temperature and finite difference results (domain size $R_\infty=Z_\infty=10,50,100$) for pure conduction case (a) R=0 and 0.99 (b) R=0.6 (c) R=0.31 and 0.80

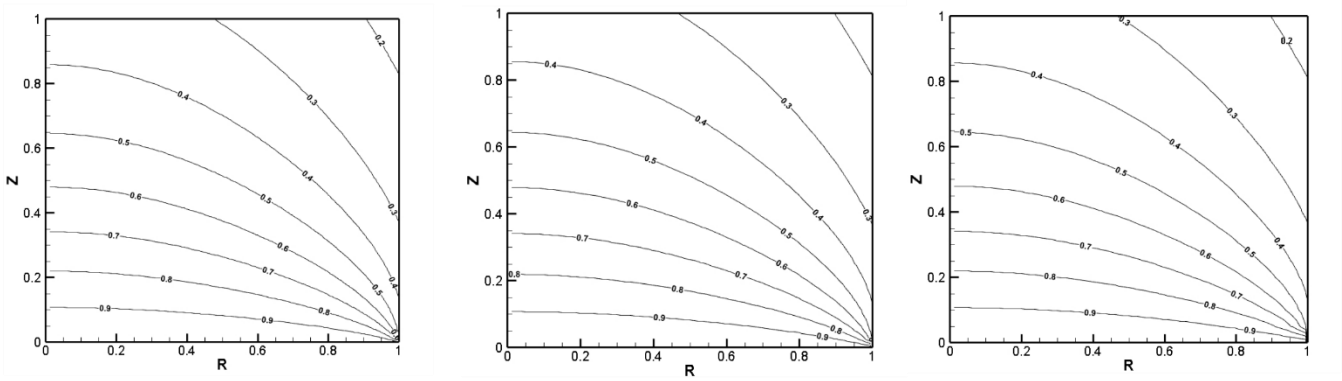

(a) $R_\infty=Z_\infty=10$ ***(b) $R_\infty=Z_\infty=50$*** ***(c) $R_\infty=Z_\infty=100$***

Figure 4-2.Isotherms over heater for various domain size (a) $R_\infty = Z_\infty = 10$ (b) $R_\infty = Z_\infty = 50$ (c) $R_\infty = Z_\infty = 100$

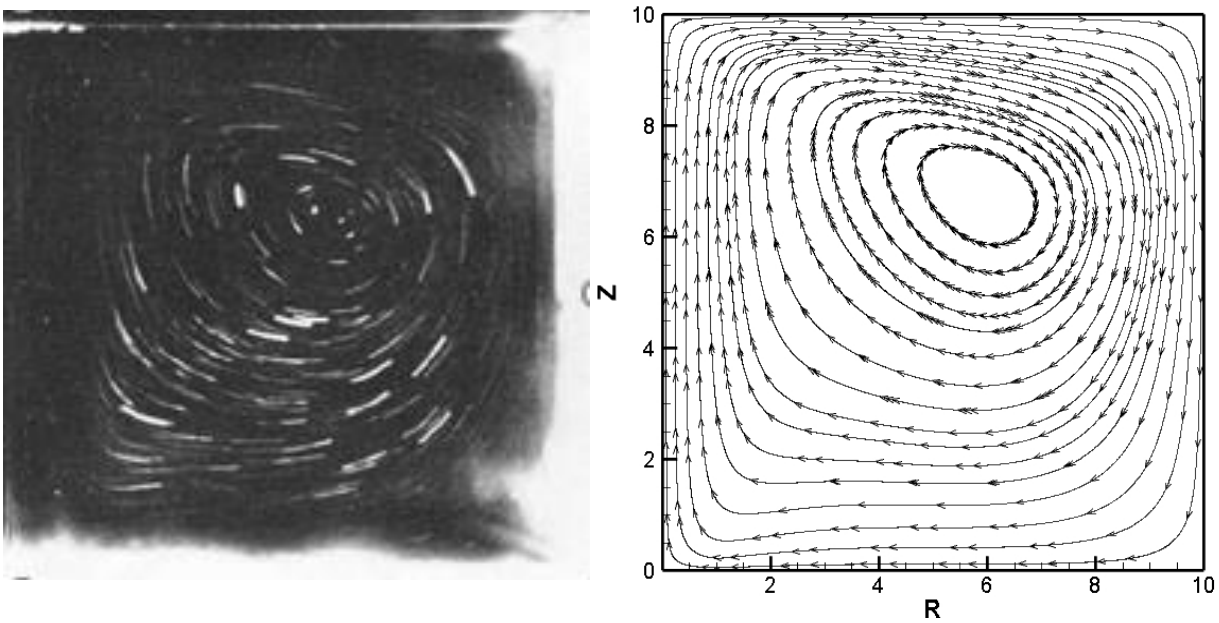

Figure 4-3. Streamline pattern in experimental study by Torrence and Orloff [29](Left) and present study by numerical modelling (Right) situation for Ra=560, Pr=0.7

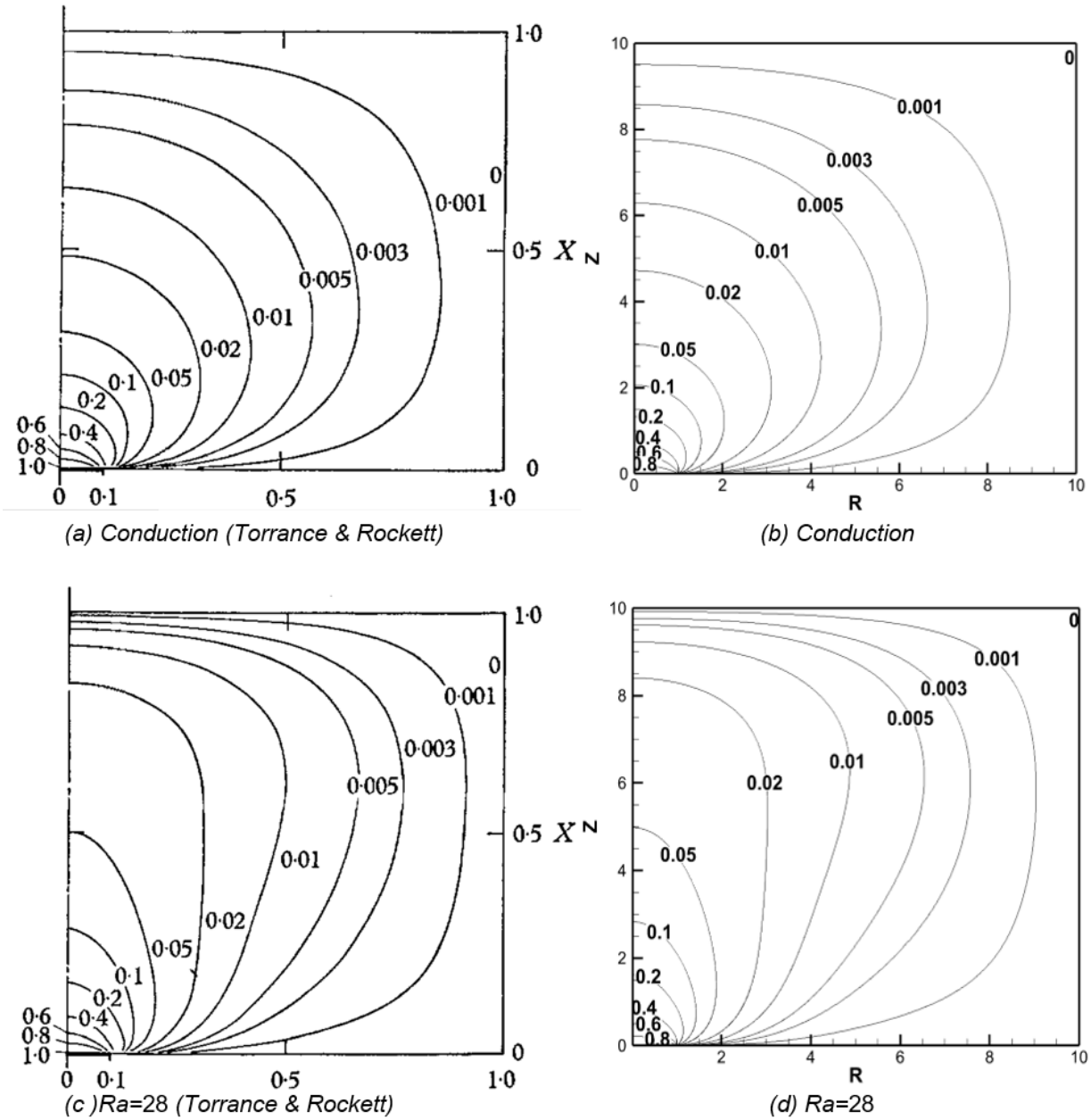

Figure 4-4. Comparison of steady state isotherms between Torrance et al. [28] and present work for Pr=0.7 (a) & (b)for case of conduction (Ra~0) (c) & (d) Ra=28

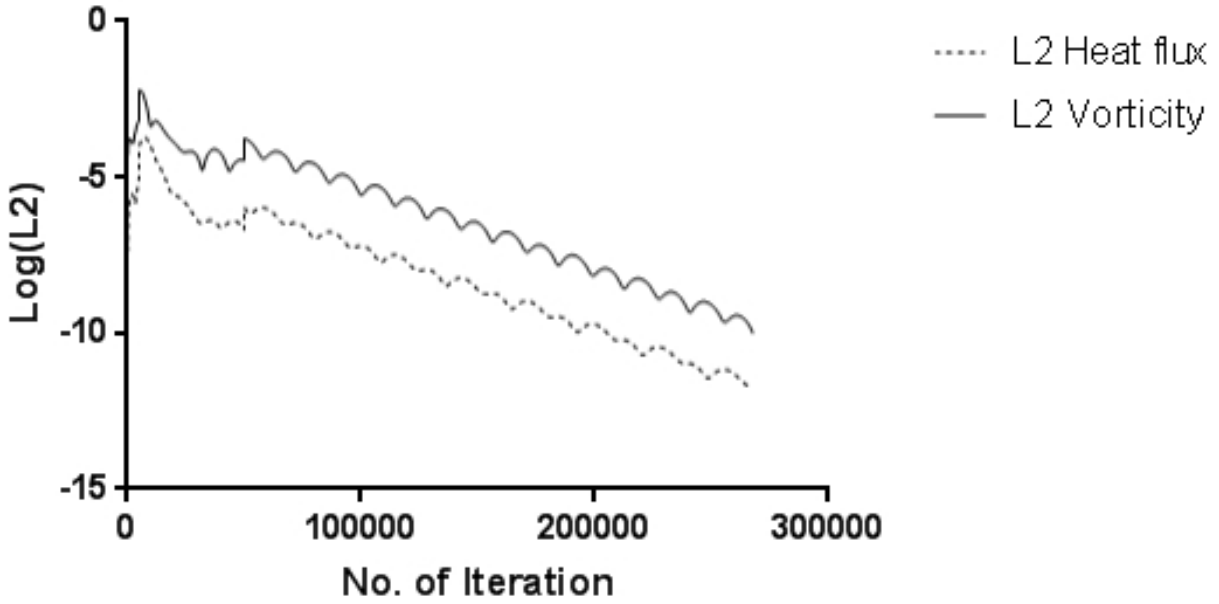

Figure 4-5. Heat flux and vorticity residual plot for Pr=10 with Ra=28 with initial condition of θ=U=V=0

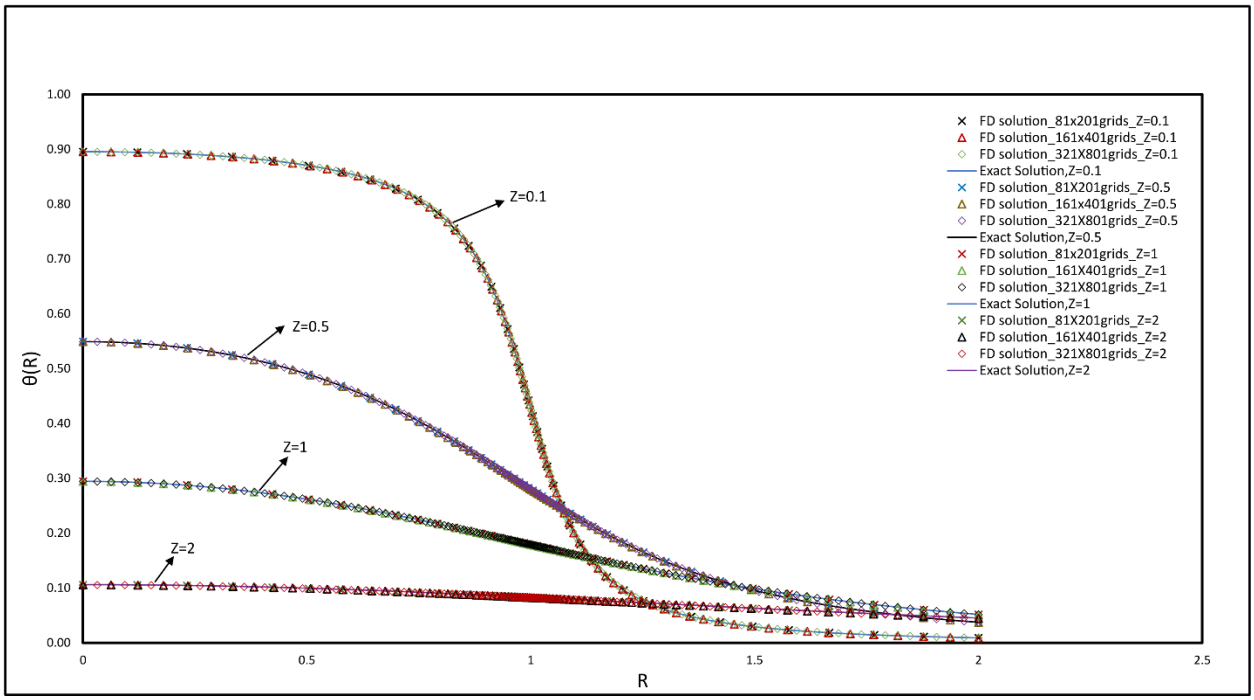

Figure 4-6. Comparison between exact solution of temperature and finite difference results for grid sizes 81X201,161X401 and 321X801 for pure conduction case

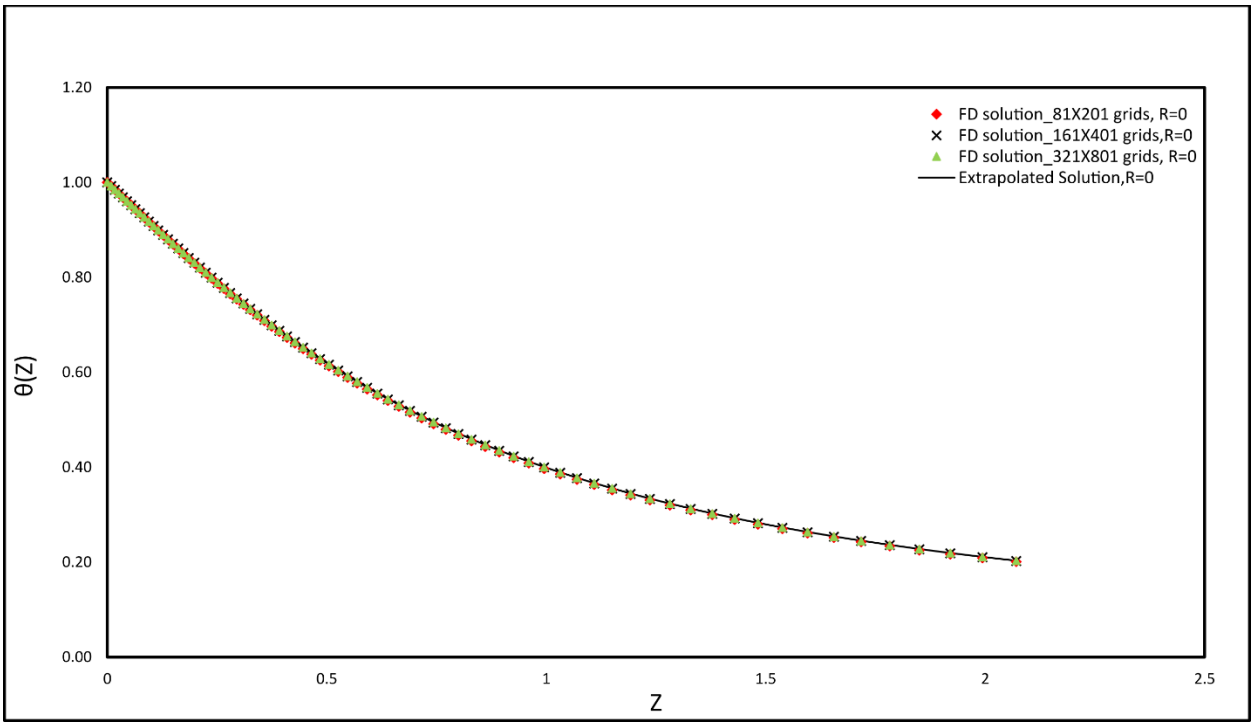

Figure 4-7. Comparison between extrapolated solution of temperature and finite difference results for grid sizes 81X201,161X401 and 321X801 at R=0 for Ra=100, Pr=1

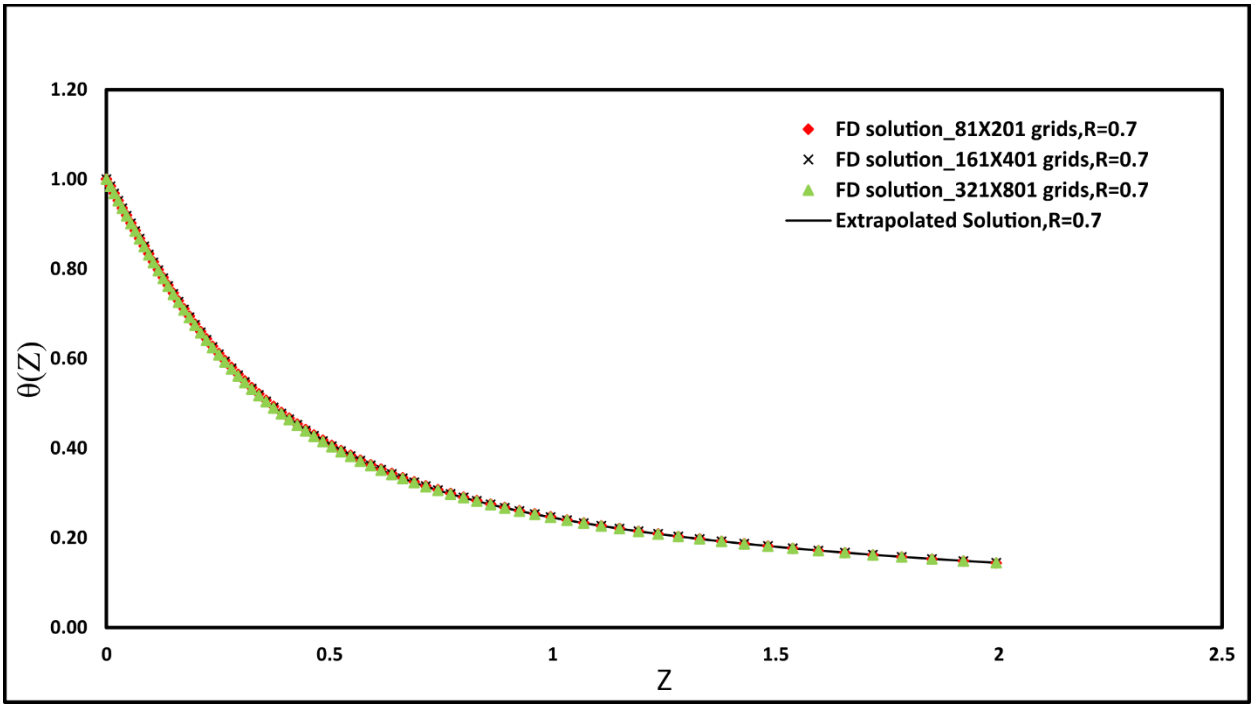

Figure 4-8. Comparison between extrapolated solution of temperature and finite difference results for grid sizes 81X201,161X401 and 321X801 at R=0.7 for Ra=100, Pr=1

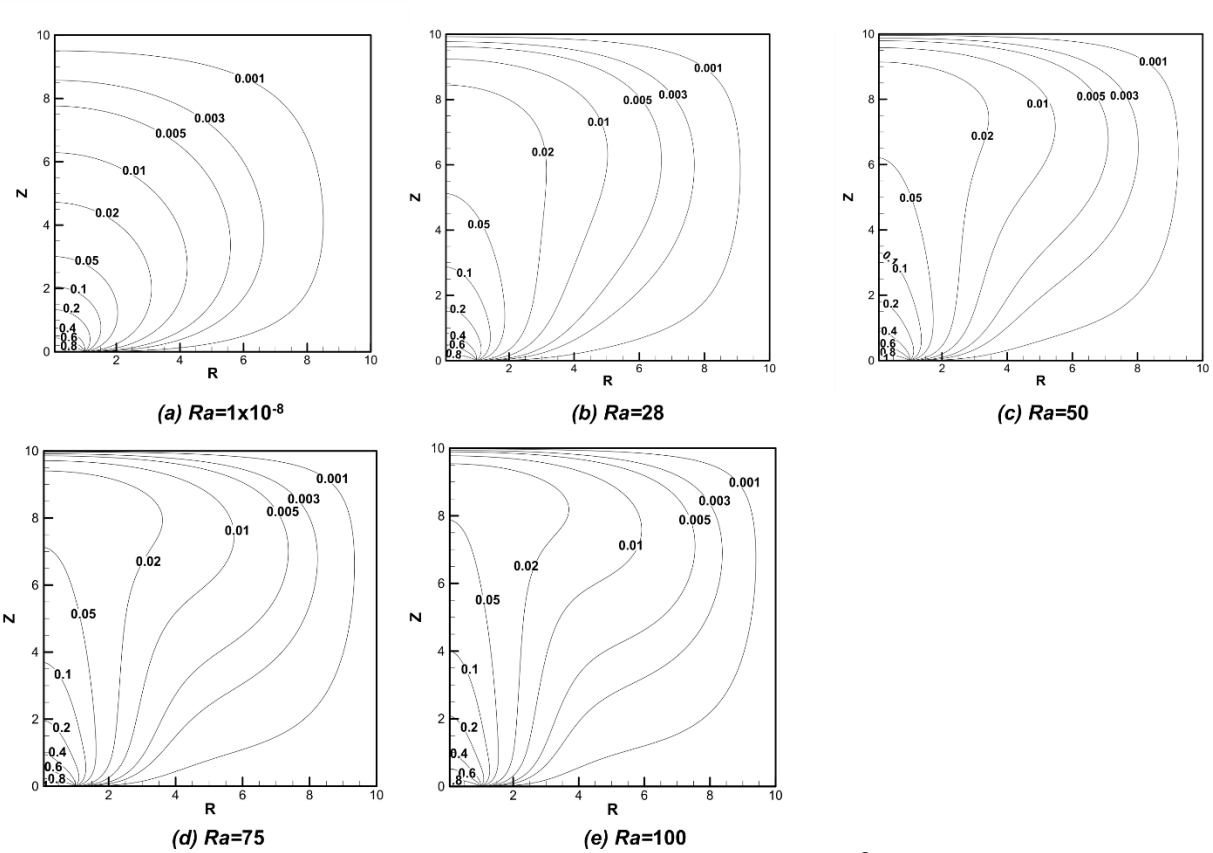

Figure 4-9. Steady state isotherms for Pr=1 with (a)Ra=1X10^{-8} (conduction) (b)Ra=28 (c) Ra=50 (d) Ra=75 (e) Ra=100

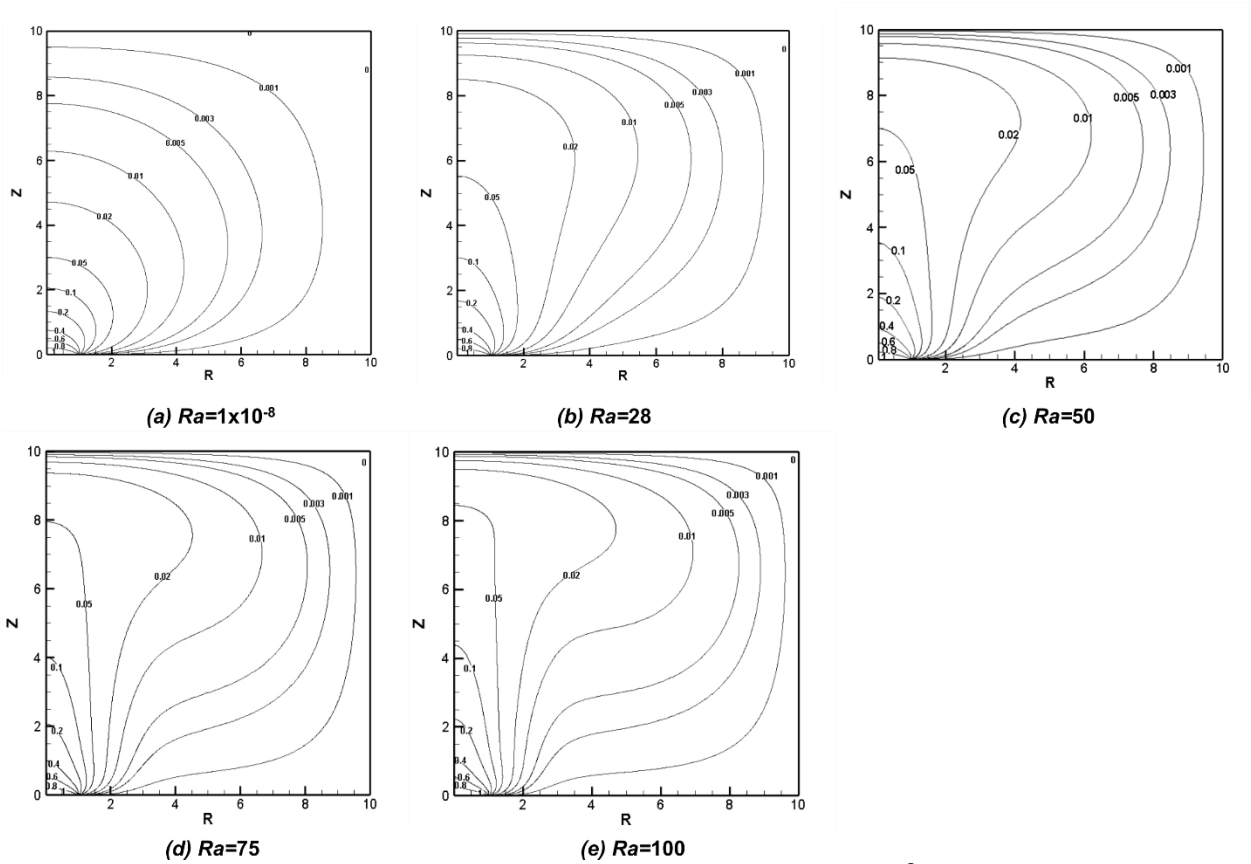

Figure 4-10. Steady state isotherms for Pr=10 with (a)Ra=1X10^{-8} (conduction) (b)Ra=28 (c) Ra=50 (d) Ra=75 (e) Ra=100

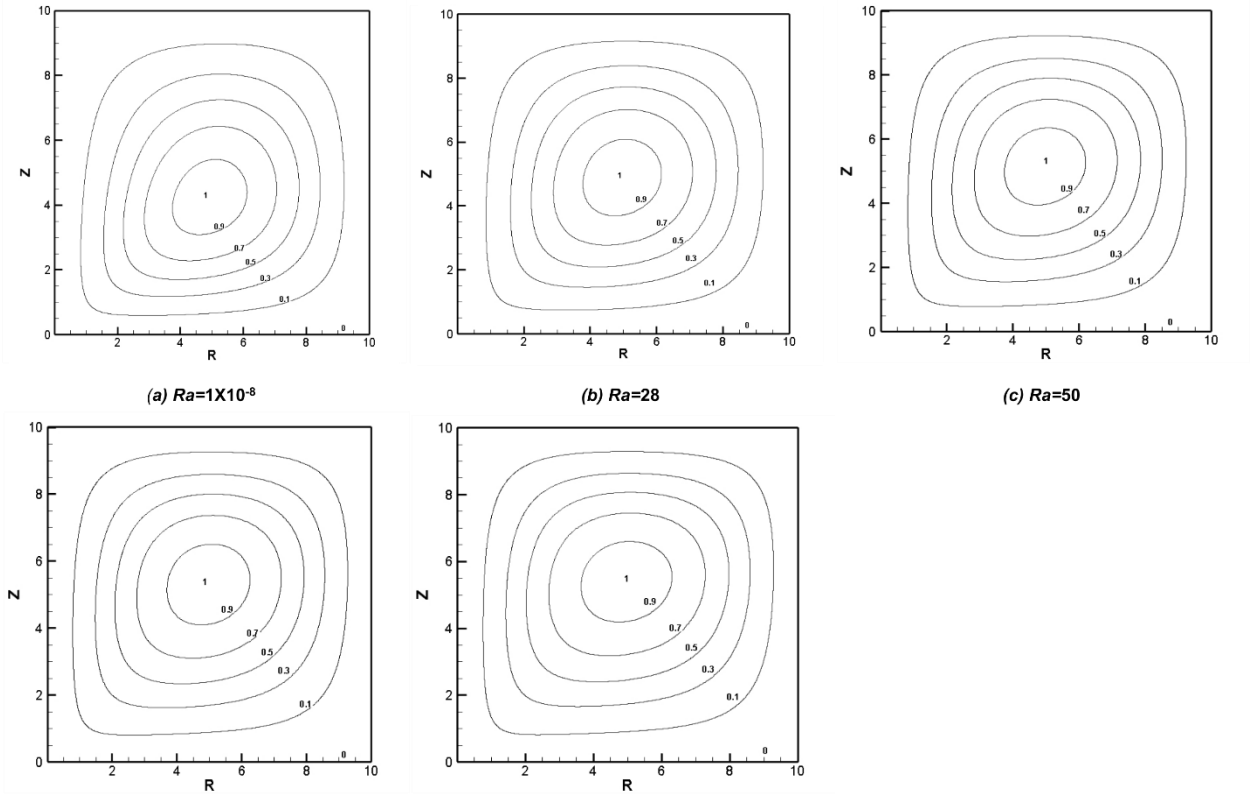

(a) Ra=1X10^{-8} *(b) Ra*=28 *(c) Ra*=50

(d) Ra=75 *(e) Ra*=100

Figure 4-11. Steady state streamlines for Pr=10 with (a)Ra=1X10^{-8} (conduction) (b)Ra=28 (c) Ra=50 (d) Ra=75 (e) Ra=100

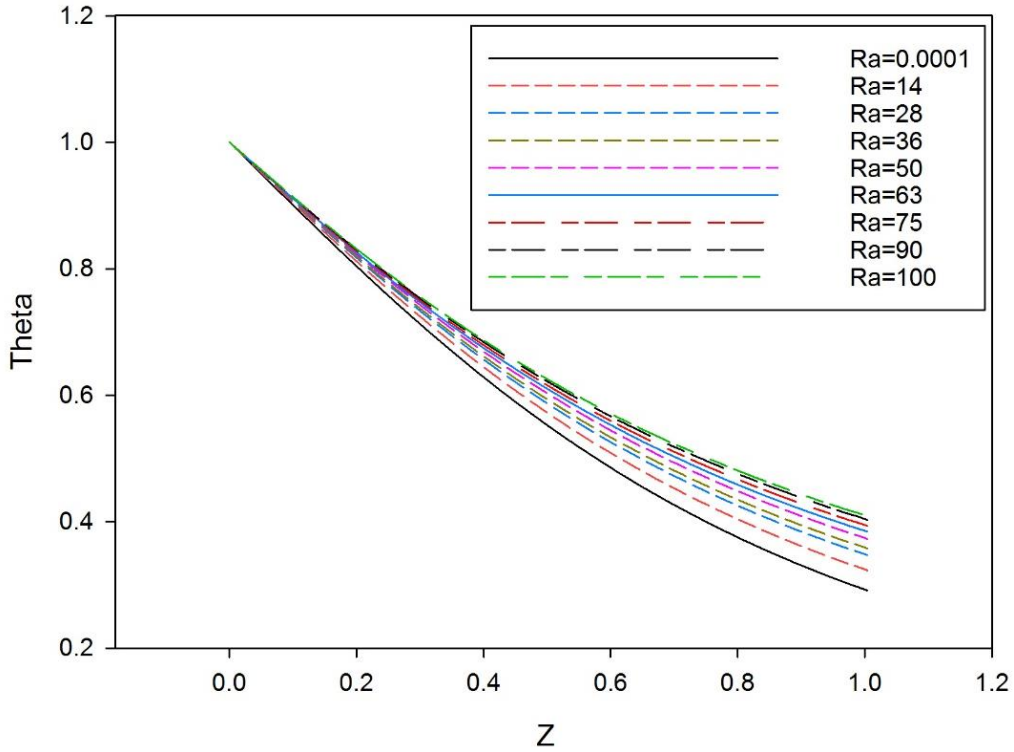

Figure 4-12.Temperature profile θ (Z, R=0) at centerline for different values of Ra at Pr=10

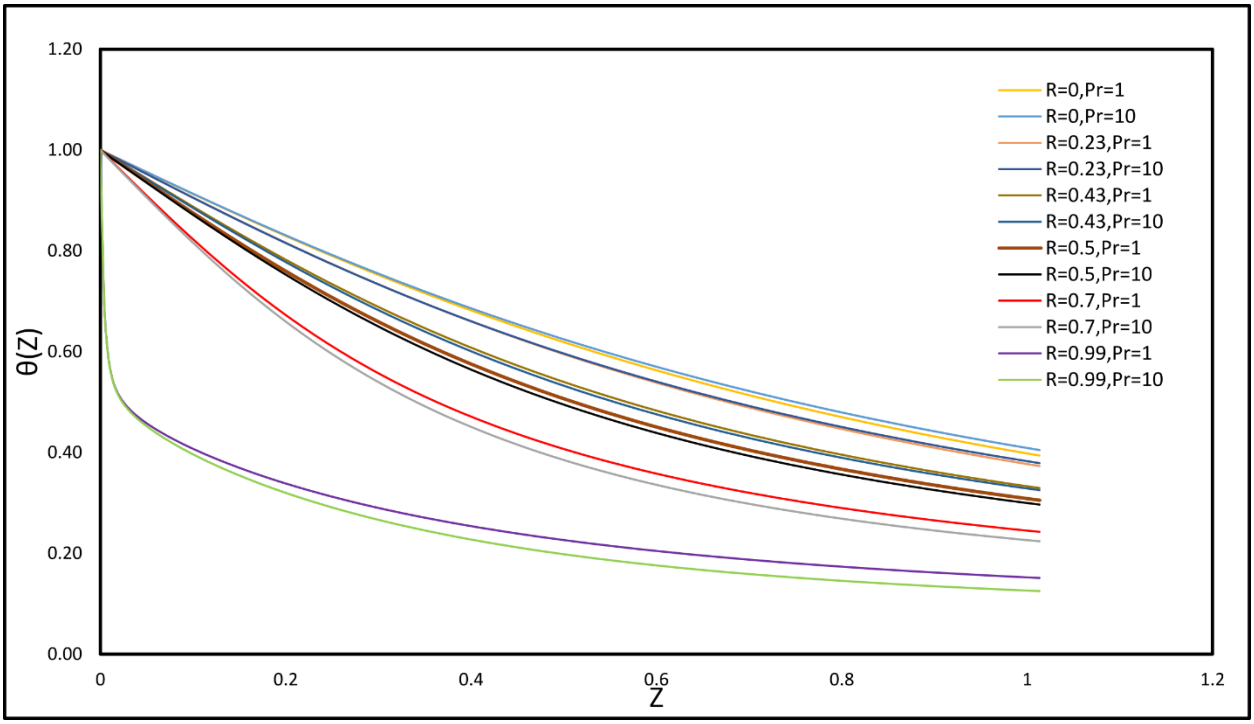

Figure 4-13.Variation of temperature in axial direction at various R locations for Ra=100 with Pr=1 and 10

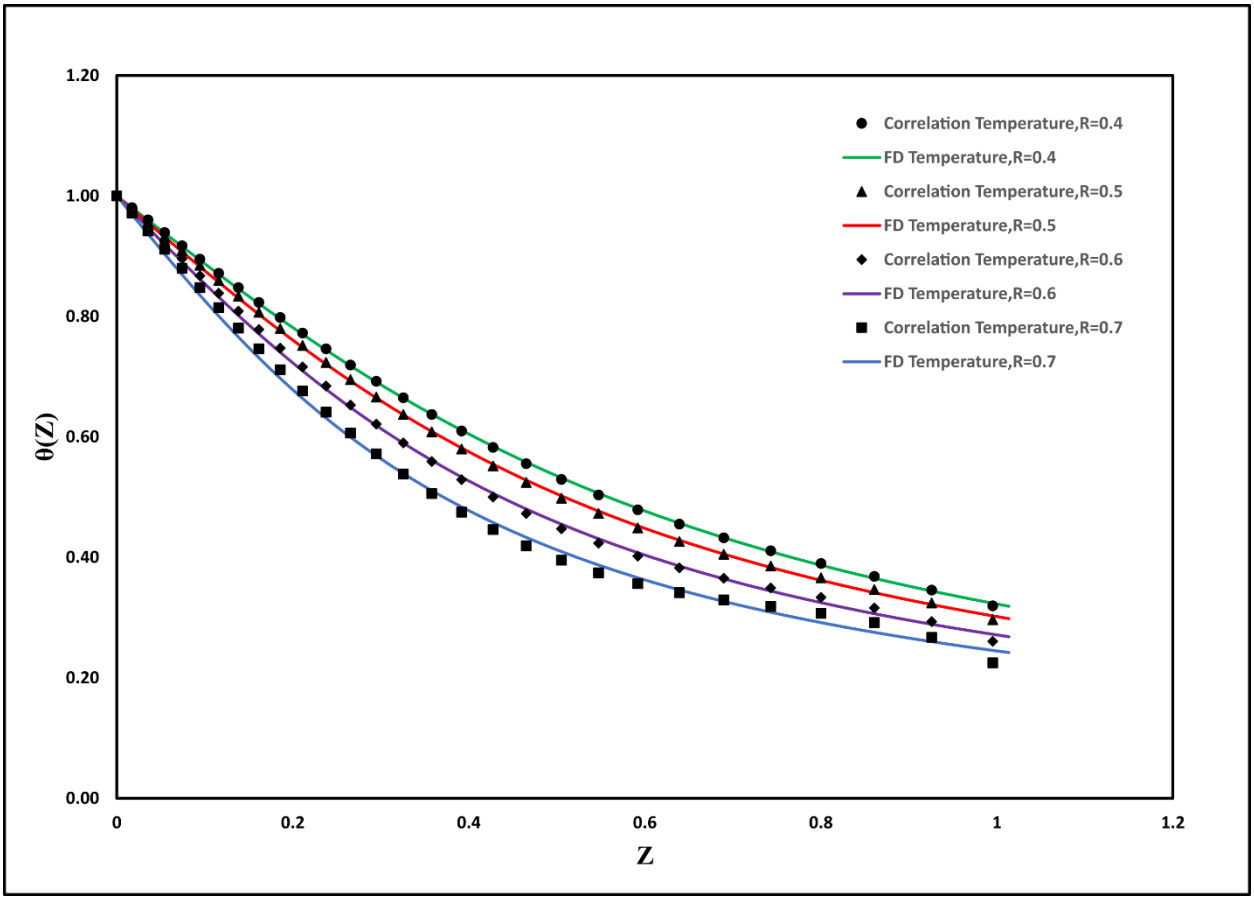

Figure 4-14. Comparison of temperature obtained by correlation and finite difference for Ra=55, Pr=10 at various radial locations

Table 4-1. Grid convergence and local order of accuracy for R=1, Z=0.026471 with Ra=100, Pr=1

Grids	Vorticity	Stream-function	Theta	U	V
321X801	8.841803	-0.003635	0.466303	-0.264470	0.002424
161X401	8.840194	-0.003636	0.466320	-0.264428	0.002424
81X201	8.833707	-0.003637	0.466393	-0.264241	0.002425
Local order of accuracy	2.011734	1.539540	2.064130	2.157078	2.588845
Extrapolated Value	8.842333	-0.003635	0.466297	-0.264482	0.002424
% deviation of 161X401 grid value from extrapolated value	0.024192	0.022781	0.004915	0.020392	0.007348

Table 4-2. Comparison of finite difference results for various grid size at R=0, with the extrapolated value for Ra=100, Pr=1

Z	(f_3)81X201 grids	(f_2)161X401 grids	(f_1)321X401 grids	p	e21	e32	GCI21	GCI32
0.00000	1.00000	1.00000	1.00000	2.0000!	0.00000	0.00000	0	0
0.00866	0.99234	0.99239	0.99240	2.30093	0.00001	0.00005	0.00000	0.00002
0.01748	0.98454	0.98464	0.98466	2.30058	0.00002	0.00010	0.00001	0.00003
0.02647	0.97659	0.97674	0.97678	2.30012	0.00003	0.00016	0.00001	0.00005
0.03564	0.96849	0.96870	0.96875	2.29956	0.00004	0.00022	0.00001	0.00007
0.04499	0.96025	0.96052	0.96057	2.29890	0.00006	0.00028	0.00002	0.00009
0.05453	0.95187	0.95219	0.95226	2.29816	0.00007	0.00034	0.00002	0.00011
0.06426	0.94333	0.94371	0.94379	2.29735	0.00008	0.00041	0.00003	0.00013
0.07419	0.93465	0.93509	0.93518	2.29647	0.00010	0.00047	0.00003	0.00015
0.08432	0.92583	0.92633	0.92643	2.29554	0.00011	0.00054	0.00004	0.00017
0.09466	0.91685	0.91742	0.91753	2.29458	0.00013	0.00062	0.00004	0.00020
0.10522	0.90773	0.90836	0.90849	2.29360	0.00014	0.00069	0.00005	0.00022
0.11600	0.89847	0.89916	0.89931	2.29263	0.00016	0.00077	0.00005	0.00025
0.12702	0.88906	0.88982	0.88998	2.29168	0.00018	0.00086	0.00006	0.00028
0.13827	0.87950	0.88034	0.88051	2.29076	0.00019	0.00095	0.00006	0.00030
0.14976	0.86981	0.87071	0.87089	2.28991	0.00021	0.00104	0.00007	0.00033
0.16151	0.85997	0.86094	0.86114	2.28914	0.00023	0.00113	0.00007	0.00036
0.17352	0.84999	0.85104	0.85125	2.28848	0.00025	0.00123	0.00008	0.00040
0.18580	0.83987	0.84099	0.84122	2.28792	0.00027	0.00133	0.00009	0.00043
0.19835	0.82962	0.83082	0.83106	2.28751	0.00030	0.00144	0.00010	0.00046
0.21120	0.81923	0.82050	0.82077	2.28725	0.00032	0.00155	0.00010	0.00050
0.22434	0.80871	0.81006	0.81034	2.28716	0.00034	0.00167	0.00011	0.00054
0.23779	0.79806	0.79949	0.79978	2.28725	0.00037	0.00179	0.00012	0.00058

0.25156	0.78729	0.78879	0.78910	2.28754	0.00039	0.00191	0.00013	0.00062
0.26566	0.77639	0.77798	0.77830	2.28805	0.00042	0.00204	0.00013	0.00066
0.28010	0.76537	0.76704	0.76738	2.28877	0.00044	0.00217	0.00014	0.00070
0.29489	0.75424	0.75598	0.75634	2.28973	0.00047	0.00231	0.00015	0.00074
0.31005	0.74299	0.74482	0.74519	2.29093	0.00050	0.00245	0.00016	0.00079
0.32558	0.73164	0.73354	0.73393	2.29237	0.00053	0.00260	0.00017	0.00083
0.34151	0.72018	0.72217	0.72257	2.29407	0.00056	0.00274	0.00018	0.00088
0.35785	0.70863	0.71069	0.71111	2.29603	0.00059	0.00290	0.00019	0.00093
0.37461	0.69699	0.69912	0.69956	2.29825	0.00062	0.00305	0.00020	0.00097
0.39180	0.68526	0.68746	0.68791	2.30073	0.00065	0.00321	0.00021	0.00102
0.40946	0.67344	0.67572	0.67619	2.30348	0.00068	0.00337	0.00022	0.00107
0.42758	0.66156	0.66391	0.66438	2.30649	0.00072	0.00354	0.00023	0.00112
0.44619	0.64960	0.65202	0.65251	2.30977	0.00075	0.00370	0.00024	0.00117
0.46532	0.63759	0.64007	0.64057	2.31331	0.00078	0.00387	0.00025	0.00122
0.48497	0.62552	0.62806	0.62857	2.31710	0.00081	0.00404	0.00025	0.00127
0.50518	0.61340	0.61600	0.61652	2.32114	0.00084	0.00421	0.00026	0.00132
0.52596	0.60125	0.60390	0.60443	2.32543	0.00087	0.00438	0.00027	0.00137
0.54733	0.58906	0.59176	0.59230	2.32995	0.00091	0.00456	0.00028	0.00141
0.56933	0.57686	0.57960	0.58014	2.33469	0.00094	0.00473	0.00029	0.00146
0.59198	0.56463	0.56741	0.56796	2.33964	0.00097	0.00490	0.00030	0.00151
0.61530	0.55240	0.55522	0.55577	2.34480	0.00100	0.00507	0.00031	0.00155
0.63932	0.54018	0.54302	0.54358	2.35013	0.00103	0.00523	0.00031	0.00160
0.66408	0.52796	0.53083	0.53139	2.35563	0.00105	0.00540	0.00032	0.00164
0.68961	0.51577	0.51865	0.51921	2.36127	0.00108	0.00556	0.00033	0.00168
0.71593	0.50360	0.50650	0.50706	2.36704	0.00111	0.00572	0.00033	0.00172
0.74309	0.49147	0.49438	0.49494	2.37290	0.00113	0.00588	0.00034	0.00176
0.77112	0.47939	0.48230	0.48286	2.37884	0.00116	0.00603	0.00034	0.00179
0.80006	0.46737	0.47027	0.47083	2.38483	0.00118	0.00617	0.00035	0.00183
0.82996	0.45541	0.45831	0.45886	2.39083	0.00120	0.00631	0.00035	0.00186
0.86085	0.44353	0.44641	0.44696	2.39681	0.00122	0.00645	0.00036	0.00189
0.89279	0.43173	0.43459	0.43513	2.40274	0.00124	0.00658	0.00036	0.00192
0.92582	0.42002	0.42286	0.42340	2.40858	0.00126	0.00671	0.00037	0.00195
0.96000	0.40842	0.41123	0.41175	2.41430	0.00128	0.00683	0.00037	0.00197
0.99537	0.39693	0.39970	0.40022	2.41986	0.00130	0.00694	0.00037	0.00199
1.03200	0.38555	0.38829	0.38879	2.42521	0.00131	0.00705	0.00038	0.00202

Table 4-3. Position of rolling vertex and value of ψmax for Pr=10

Ra	Z	R	Ψ max
0	4.204	4.938	1.497E-05
28	4.894	4.938	7.796
50	5.169	4.938	13.637
75	5.338	4.938	18.510
100	5.443	4.938	22.316

Table 4-4. Polynomial coefficients in developing correlation for Pr=1

a_1	a_3	a_4	R	Ra
-0.99960	0.54471	-0.25315	0.00000	0
-1.00231	0.55103	-0.25730	0.06278	0
-1.01042	0.57001	-0.26975	0.12269	0
-1.02334	0.60072	-0.29002	0.17983	0
-1.04072	0.64302	-0.31820	0.23425	0
-1.06234	0.69717	-0.35467	0.28604	0
-1.08804	0.76370	-0.40000	0.33525	0
-1.11773	0.84333	-0.45495	0.38198	0
-1.15134	0.93689	-0.52036	0.42627	0
-1.18881	1.04527	-0.59710	0.46822	0
-1.23010	1.16932	-0.68606	0.50790	0
-1.27515	1.30985	-0.78807	0.54536	0
-1.32385	1.46751	-0.90384	0.58070	0
-1.37610	1.64276	-1.03396	0.61397	0
-1.43175	1.83583	-1.17879	0.64525	0
-1.49058	2.04666	-1.33847	0.67462	0
-1.55237	2.27486	-1.51285	0.70214	0
-0.96154	0.54481	-0.26156	0.00000	14
-0.96455	0.55142	-0.26584	0.06278	14
-0.97359	0.57128	-0.27866	0.12269	14
-0.98795	0.60340	-0.29956	0.17983	14
-1.00721	0.64763	-0.32862	0.23425	14
-1.03108	0.70421	-0.36624	0.28604	14
-1.05933	0.77368	-0.41305	0.33525	14
-1.09183	0.85675	-0.46980	0.38198	14
-1.12844	0.95425	-0.53734	0.42627	14
-1.16905	1.06702	-0.61657	0.46822	14
-1.21358	1.19591	-0.70836	0.50790	14
-1.26191	1.34167	-0.81352	0.54536	14
-1.31392	1.50489	-0.93276	0.58070	14

-1.36944	1.68598	-1.06659	0.61397	14
-1.42830	1.88509	-1.21535	0.64525	14
-1.49026	2.10206	-1.37911	0.67462	14
-1.55505	2.33644	-1.55766	0.70214	14
-0.93584	0.54792	-0.27001	0.00000	28
-0.93916	0.55481	-0.27440	0.06278	28
-0.94914	0.57550	-0.28757	0.12269	28
-0.96495	0.60896	-0.30904	0.17983	28
-0.98611	0.65503	-0.33893	0.23425	28
-1.01223	0.71395	-0.37765	0.28604	28
-1.04305	0.78625	-0.42586	0.33525	28
-1.07833	0.87264	-0.48434	0.38198	28
-1.11791	0.97393	-0.55395	0.42627	28
-1.16162	1.09096	-0.63559	0.46822	28
-1.20932	1.22453	-0.73014	0.50790	28
-1.26085	1.37535	-0.83838	0.54536	28
-1.31604	1.54396	-0.96099	0.58070	28
-1.37471	1.73068	-1.09845	0.61397	28
-1.43663	1.93559	-1.25103	0.64525	28
-1.50155	2.15846	-1.41875	0.67462	28
-1.56916	2.39873	-1.60134	0.70214	28
-0.92438	0.54968	-0.27424	0.00000	36
-0.92787	0.55672	-0.27869	0.06278	36
-0.93835	0.57785	-0.29205	0.12269	36
-0.95495	0.61203	-0.31383	0.17983	36
-0.97713	0.65909	-0.34416	0.23425	36
-1.00446	0.71926	-0.38348	0.28604	36
-1.03665	0.79308	-0.43244	0.33525	36
-1.07342	0.88126	-0.49185	0.38198	36
-1.11458	0.98459	-0.56259	0.42627	36
-1.15993	1.10392	-0.64554	0.46822	36
-1.20929	1.24001	-0.74159	0.50790	36
-1.26250	1.39354	-0.85151	0.54536	36
-1.31936	1.56504	-0.97595	0.58070	36
-1.37966	1.75478	-1.11537	0.61397	36
-1.44317	1.96279	-1.27002	0.64525	36
-1.50961	2.18879	-1.43986	0.67462	36
-1.57867	2.43220	-1.62461	0.70214	36
-0.90765	0.55277	-0.28093	0.00000	50

-0.91142	0.56006	-0.28548	0.06278	50
-0.92274	0.58193	-0.29913	0.12269	50
-0.94065	0.61730	-0.32142	0.17983	50
-0.96452	0.66599	-0.35248	0.23425	50
-0.99387	0.72825	-0.39279	0.28604	50
-1.02832	0.80460	-0.44303	0.33525	50
-1.06755	0.89575	-0.50401	0.38198	50
-1.11129	1.00249	-0.57663	0.42627	50
-1.15932	1.12563	-0.66180	0.46822	50
-1.21141	1.26591	-0.76036	0.50790	50
-1.26735	1.42397	-0.87309	0.54536	50
-1.32691	1.60025	-1.00059	0.58070	50
-1.38985	1.79499	-1.14329	0.61397	50
-1.45590	2.00812	-1.30138	0.64525	50
-1.52478	2.23930	-1.47477	0.67462	50
-1.59615	2.48785	-1.66311	0.70214	50
-0.89486	0.55565	-0.28649	0.00000	63
-0.89888	0.56315	-0.29112	0.06278	63
-0.91095	0.58566	-0.30504	0.12269	63
-0.93000	0.62208	-0.32777	0.17983	63
-0.95535	0.67220	-0.35948	0.23425	63
-0.98646	0.73629	-0.40066	0.28604	63
-1.02288	0.81486	-0.45202	0.33525	63
-1.06425	0.90863	-0.51440	0.38198	63
-1.11024	1.01836	-0.58870	0.42627	63
-1.16058	1.14486	-0.67582	0.46822	63
-1.21501	1.28882	-0.77662	0.50790	63
-1.27328	1.45085	-0.89184	0.54536	63
-1.33514	1.63133	-1.02205	0.58070	63
-1.40031	1.83042	-1.16765	0.61397	63
-1.46851	2.04801	-1.32876	0.64525	63
-1.53943	2.28369	-1.50527	0.67462	63
-1.61273	2.53670	-1.69674	0.70214	63
-0.88480	0.55827	-0.29117	0.00000	75
-0.88904	0.56596	-0.29589	0.06278	75
-0.90175	0.58903	-0.31003	0.12269	75
-0.92181	0.62636	-0.33316	0.17983	75
-0.94847	0.67775	-0.36544	0.23425	75
-0.98112	0.74345	-0.40739	0.28604	75

-1.01926	0.82398	-0.45975	0.33525	75
-1.06249	0.92006	-0.52337	0.38198	75
-1.11043	1.03244	-0.59916	0.42627	75
-1.16278	1.16190	-0.68803	0.46822	75
-1.21924	1.30911	-0.79081	0.50790	75
-1.27952	1.47463	-0.90824	0.54536	75
-1.34334	1.65879	-1.04086	0.58070	75
-1.41042	1.86171	-1.18901	0.61397	75
-1.48045	2.08321	-1.35280	0.64525	75
-1.55310	2.32281	-1.53204	0.67462	75
-1.62803	2.57969	-1.72627	0.70214	75
-0.87400	0.56148	-0.29654	0.00000	90
-0.87849	0.56939	-0.30135	0.06278	90
-0.89198	0.59313	-0.31577	0.12269	90
-0.91325	0.63155	-0.33936	0.17983	90
-0.94146	0.68445	-0.37232	0.23425	90
-0.97594	0.75207	-0.41520	0.28604	90
-1.01613	0.83495	-0.46876	0.33525	90
-1.06155	0.93379	-0.53388	0.38198	90
-1.11180	1.04934	-0.61147	0.42627	90
-1.16650	1.18234	-0.70245	0.46822	90
-1.22532	1.33344	-0.80763	0.50790	90
-1.28794	1.50312	-0.92772	0.54536	90
-1.35405	1.69167	-1.06322	0.58070	90
-1.42334	1.89914	-1.21444	0.61397	90
-1.49548	2.12527	-1.38142	0.64525	90
-1.57012	2.36950	-1.56392	0.67462	90
-1.64690	2.63095	-1.76143	0.70214	90
-0.86766	0.56356	-0.29986	0.00000	100
-0.87233	0.57162	-0.30472	0.06278	100
-0.88632	0.59578	-0.31932	0.12269	100
-0.90835	0.63490	-0.34321	0.17983	100
-0.93755	0.68876	-0.37661	0.23425	100
-0.97320	0.75762	-0.42010	0.28604	100
-1.01469	0.84201	-0.47444	0.33525	100
-1.06151	0.94263	-0.54052	0.38198	100
-1.11321	1.06022	-0.61928	0.42627	100
-1.16940	1.19549	-0.71162	0.46822	100
-1.22971	1.34908	-0.81835	0.50790	100

-1.29380	1.52143	-0.94015	0.54536	100
-1.36135	1.71279	-1.07752	0.58070	100
-1.43201	1.92316	-1.23071	0.61397	100
-1.50546	2.15223	-1.39974	0.64525	100
-1.58133	2.39941	-1.58433	0.67462	100
-1.65925	2.66375	-1.78392	0.70214	100

Table 4-5. Comparison between heat flux given by correlation and finite difference for the case of Ra=28, Pr=10

R	b_1	Q	% Difference
0.00000	0.93560	0.93966	0.43404
0.04969	0.93792	0.93705	0.09286
0.11180	0.94745	0.94600	0.15259
0.17391	0.96466	0.96506	0.04180
0.24845	0.99641	0.99859	0.21906
0.33540	1.05122	1.05268	0.13877
0.42236	1.13021	1.12910	0.09852
0.53416	1.28302	1.28204	0.07675

CHAPTER 5
CONCLUSIONS

Steady state, laminar, external natural convection flow over an isothermal, circular microheater is studied for Rayleigh number range up to 100 at Prandtl number of 1,5 and 10. Finite difference scheme is used to model the fluid flow over heater. Influence of domain size is observed on the flow field near the heater for pure conduction case. Grid dependence studies for the case of pure conduction and moderate convective flows are conducted by extrapolating the finite difference results using Richardson extrapolation. Results obtained by finite difference are fitted using least square regression fit to obtain a correlation for temperature field near heater. Three 4^{th} order unified polynomials are developed to describe dimensionless temperature field near heater; each for the case of Pr=1,5 and 10. This temperature field is of the form θ (Z, R, Ra) for any given Pr; where $0 \leq Ra \leq 100$ and $0 \leq Z \leq 1; 0 \leq R \leq 0.7$. The correlation obtained is checked for Ra=55, Pr=10 with the finite difference solutions of temperature and it was also checked against wall heat flux obtained by finite difference solution for Ra=28, Pr=10. Results obtained by correlation shows good agreement with finite difference results.

The effect of Pr on temperature gradient in axial direction for a fixed Ra shows that the flow follows a boundary layer type behavior for $0.3 \leq R \leq 1$, whereas the flow does not follow boundary layer behavior in region $0 \leq R \leq 0.3$ where the fluid rises upward away from the heater wall due to convection.

LIST OF REFERENCES

[1] J. Barber, D. Brutin and L. Tadrist, "A review on boiling heat transfer enhancement with nanofluids," *Nanoscale Research Letters,* vol. 6, no. 1, p. 280, 2011.

[2] S. M. You, S. T. W and A. Bar-Cohen, "A Technique for Enhancing Boiling Heat Transfer with Application to Cooling of Electronic Equipment," *IEEE transactions on components, hybrids and manufacturing technology,* vol. 15, no. 5, pp. 823-831, 1992.

[3] N. Petralanda, "Nucleate Boiling Incipience Over Metallic/Non-Metallic Surfaces," PhD. thesis,University of Florida, Gainesville, 2015.

[4] V. K. Dhir, "Boiling heat transfer," *Annual Review Fluid Mechancs,* vol. 30, pp. 365-401, 1998.

[5] W. Porteous and M. Blander, " Limits of superheat and explosive boiling of light hydrocarbons, halocarbons, and hydrocarbon mixtures," *AIChE Journal,* vol. 21, no. 3, pp. 560-566, 1975.

[6] M. Blander and J. L. Katz, "Bubble nucleation in liquids," *AIChE Journal,* vol. 21, no. 5, pp. 833-848, 1979.

[7] C. T. Avedisian, "The Homogeneous Nucleation Limits of Liquids," *Journal of Physical and Chemical Reference Data,* vol. 14, no. 3, 1985.

[8] T. Theofanous, J. Tu, A. Dinh and T. Dinh, "The boiling crisis phenomenon:Part I: nucleation and nucleate boiling heat transfer," *Experimental Thermal and Fluid Science,* vol. 26, no. 6, pp. 775-792, 2002.

[9] Y. Qi and J. F. Klausner, "Comparison of Nucleation Site Density for Pool Boiling and Gas Nucleation," *ASME. J. Heat Transfer,* vol. 128, no. 1, pp. 13-20, 2005.

[10] B. Bon, C.-K. Guan and J. F. Klausner, "Heterogeneous nucleation on ultra smooth surfaces," *Experimental Thermal and Fluid Science,* vol. 35, no. 5, pp. 746-752, 2011.

[11] H. T. Phan, N. Caney, P. Marty, S. Colasson and J. Gavillet, "Surface wettability control by nanocoating: The effects on pool boiling heat transfer and nucleation mechanism," *International Journal of Heat and Mass Transfer,* vol. 52, no. 23, pp. 5459-5471, 2009.

[12] T. Chen, J. F. Klausner, S. V. Garimella and J. N. Chung, "Subcooled boiling incipience on a highly smooth microheater," *International Journal of Heat and Mass Transfer,* vol. 49, no. 23, pp. 4399-4406, 2006.

[13] H. Jo, H. S. Ahn, S. Kang and M. H. Kim, "A study of nucleate boiling heat transfer on hydrophilic, hydrophobic and heterogeneous wetting surfaces," *International Journal of Heat and Mass Transfer,* vol. 54, no. 25, pp. 5643-5652, 2011.

[14] H. Jo, S. Kim, H. Kim, J. Kim and M. H. Kim, "Nucleate boiling performance on nano/microstructures with different wetting surfaces," *Nanoscale Res Lett.,* vol. 7, pp. 1-9, 2012.

[15] H. Jo, M. Kaviany, S. H. Kim and M. H. Kim, "Heterogeneous bubble nucleation on ideally-smooth horizontal heated surface," *International Journal of Heat and Mass Transfer,* vol. 71, pp. 149-157, 2014.

[16] R. J. Goldstein and K.-S. Lau, "Laminar natural convection from a horizontal plate andt the influence of plate-edge extensions," *J. Fluid Mech.,* vol. 129, pp. 55-75, 1983.

[17] M. Zakerullah and J. A. D. Ackroyd, "Laminar natural convection boundary layers on horizontal circular discs," *Journal of Applied Mathematics and Physics,* vol. 30, no. 3, pp. 427-435, 1979.

[18] F. J. Suriano and Y. Kwang-Tzu, "Laminar free convection about vertical and horizontal plates at small and moderate grashof numbers," *International Journal of Heat and Mass Transfer,* vol. 11, no. 3, pp. 473-490, 1968.

[19] K. Stewartson, "On the free convection from a horizontal plate," *Journal of Applied Mathematics and Physics,* vol. 9a, pp. 276-282, 1958.

[20] W. N. Gill, D. W. Zeh and E. Casal, "Free convection on a horizontal plate," *Journal of Applied Mathematics and Physics,* vol. 16, no. 4, pp. 539-541, 1965.

[21] Z. Rotem and L. C. u. h. surfaces, "Natural convection above," *J. fluid mech.,* vol. 38, no. 1, pp. 173-192, 1969.

[22] M. Corcione, "Heat transfer correlations for free convection from upward-facing horizontal rectangular surfaces," *WSEAS TRANSACTIONS on HEAT and MASS TRANSFER,* 2007.

[23] M. Kostoglou, S. P. Evgenidis, K. A. Zacharias and T. D. Karapantsios, "Heat transfer from small objects in microgravity: Experiments and analysis," *International Journal of Heat and Mass Transfer,* vol. 54, no. 15, pp. 3323-3333, 2011.

[24] M. Kostoglou, S. P. Evgenidis and T. D. Karapantsios, "Unexpected natural convection heat transfer for small Rayleigh numbers in external geometry," *International Journal of Heat and Mass Transfer,* vol. 64, pp. 773-782, 2013.

[25] M. V. Gunaji, R. J. Pederson and I. H. Leslie, "Numerical Study of Natural Convection Over a Finite Heated Disc," in *Fundamentals of Natural Convection HTD*, 1990.

[26] M. Yovanovich and K. Jafarpur, "Bounds on laminar natural convection from isothermal disks and finite plates of arbitrary shape of all orientations and Prandtl numbers," in *Session on fundamentals of natural convection*, New Orleans, LA, 1993.

[27] T. Rule, J. Kim and T. Kalkur, "Design, construction, and qualification of a microscale heater array for use in boiling heat transfer," NASA, 1998.

[28] K. E. Torrance and J. A. Rockett, "Numerical study of natural convection in an enclosure with localized heating from below-creeping flow to the onset of laminar instability," *J. Fluid Mech.,* vol. 36, no. 1, pp. 33-54, 1969.

[29] K. E. Torrance, L. Orloff and J. A. Rockett, "Experiments on natural convection in enclosures with localized heating from below," *J. Fluid Mech.,* vol. 36, no. 1, pp. 21-31, 1969.

[30] P. J. Roache, "A Method for Uniform Reporting of Grid Refinement Studies," *J. Fluids Eng,* vol. 116, no. 3, pp. 405-413, 1994.

BIOGRAPHICAL SKETCH

Shantanu Singh was born in Lucknow, India in 1990. He obtained his Bachelor of Technology in Mechanical Engineering from Indian Institute of Technology, (BHU) Varanasi (IIT-Varanasi(BHU)), India in May 2013. Thereafter, he worked in Bharat Petroleum Corporation Limited (BPCL), India; as Research & Development engineer till August 2015. He joined the graduate program at the University of Florida in August 2015. He has been working under Dr. Renwei Mei in the Department of Mechanical and Aerospace Engineering to obtain his Master of Science degree. His current research interest includes computational fluid dynamics and scientific computing.